CHAPTER IV

RESULTS AND DISCUSSIONS

4.1 Characterizations of Raw Materials

Physical properties, compositions, phases, thermal behaviors and microstructures of the raw materials, i.e., RHA, WS and SRM30, are monitored. The information obtained is useful for sample preparation and interpretation in the following sections.

4.1.1 Density, Particle Size and Size Distribution

Size distributions of RHA, WS and SRM30 are given in Figure 4.1. Average particle sizes and densities of the raw materials are summarized in Table 4.1. The average particle size of RHA is largest. The size distribution of RHA is in a range of 0.7-90 μm, while that of SRM30 shows a bimodal curve with peaks at 0.3 and 1.5 μm in a range of 0.07-40 μm and WS has a broadest size range between 0.06-100 μm.

Table 4.1 Density and average particle size of the raw materials.

Raw materials	Density (g/cm^3)	Average particle size (μm)
RHA	2.18±0.02	17.27±0.19
WS	2.41±0.01	7.83±0.02
SRM30	3.88*	6.09±0.04

* From Loxley public company limited specification.

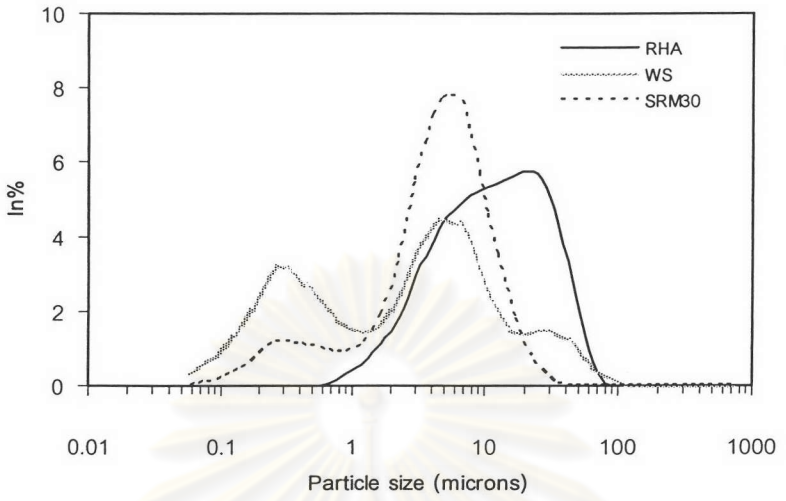

Figure 4.1 Particle size distributions of raw materials.

4.1.2 Composition and Phase

From the XRF analysis, RHA consists of 97.08 % SiO_2 and oxides of alkali and alkaline earth elements, especially K_2O (Table 4.2). The major components are silica in forms of cristobalite, quartz and amorphous silica (Figure 4.2).

Table 4.2 %Oxide contents of RHA from XRF analysis (see APPENDIX A for detail).

oxide	Na_2O	MgO	$Al(OH)_3$	SiO_2	P_2O_5	K_2O	CaO	Fe_2O_3	WO_3	Total
normalized %	0.15	0.60	0.13	97.08	0.02	1.27	0.68	0.07	0.001	100

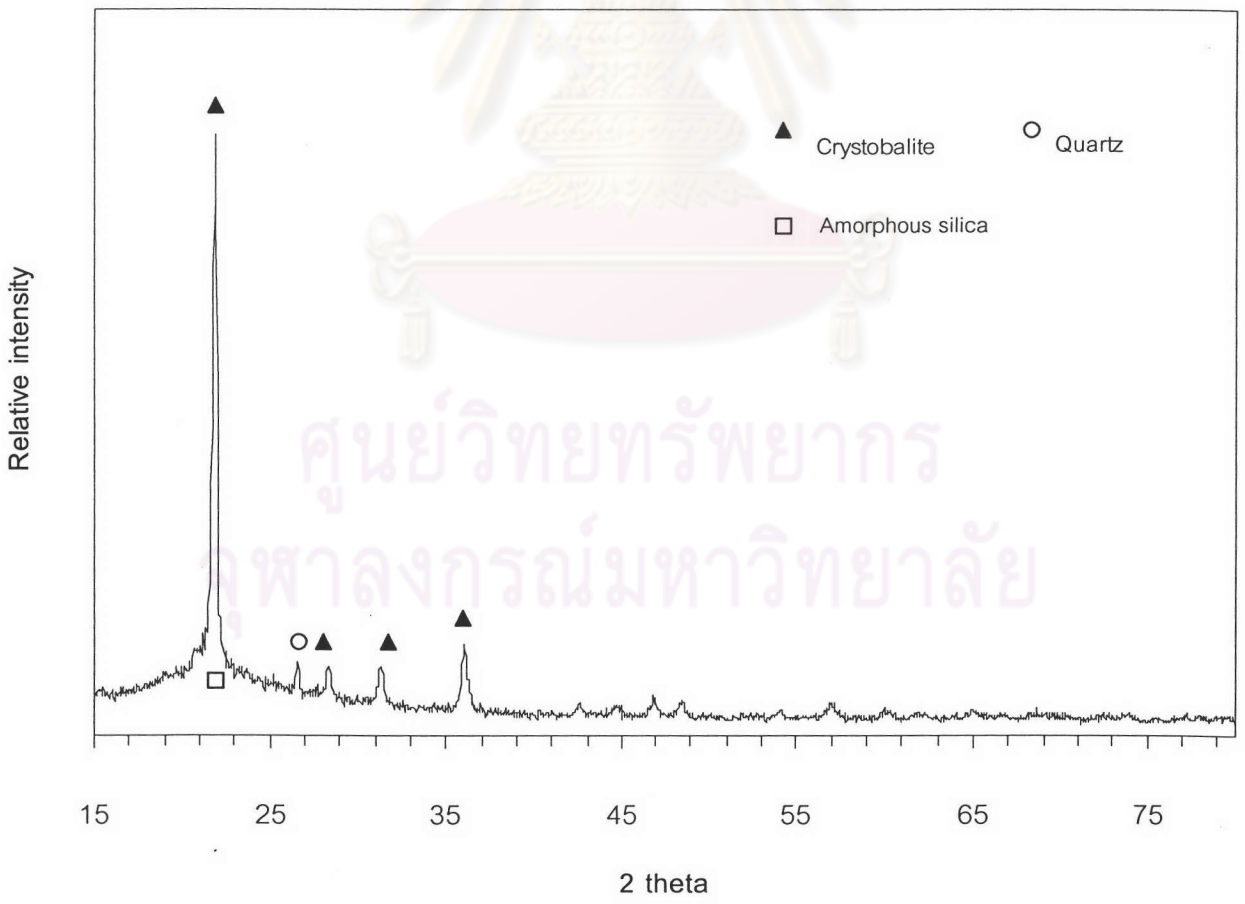

Figure 4.2 XRD pattern of RHA.

From XRD spectrum of WS, the major phase is gibbsite ($Al(OH)_3$). XRF result (Table 4.3) shows high content of $Al(OH)_3$ up to 98.19% and small amount of oxides.

Table 4.3 %Oxide contents of WS from XRF analysis (see APPENDIX A for detail).

oxide	Na_2O	MgO	Al_2O_3	SiO_2	CaO	Fe_2O_3	SnO_2	Total
normalized %	0.65	0.31	98.19	0.66	0.06	0.09	0.04	100

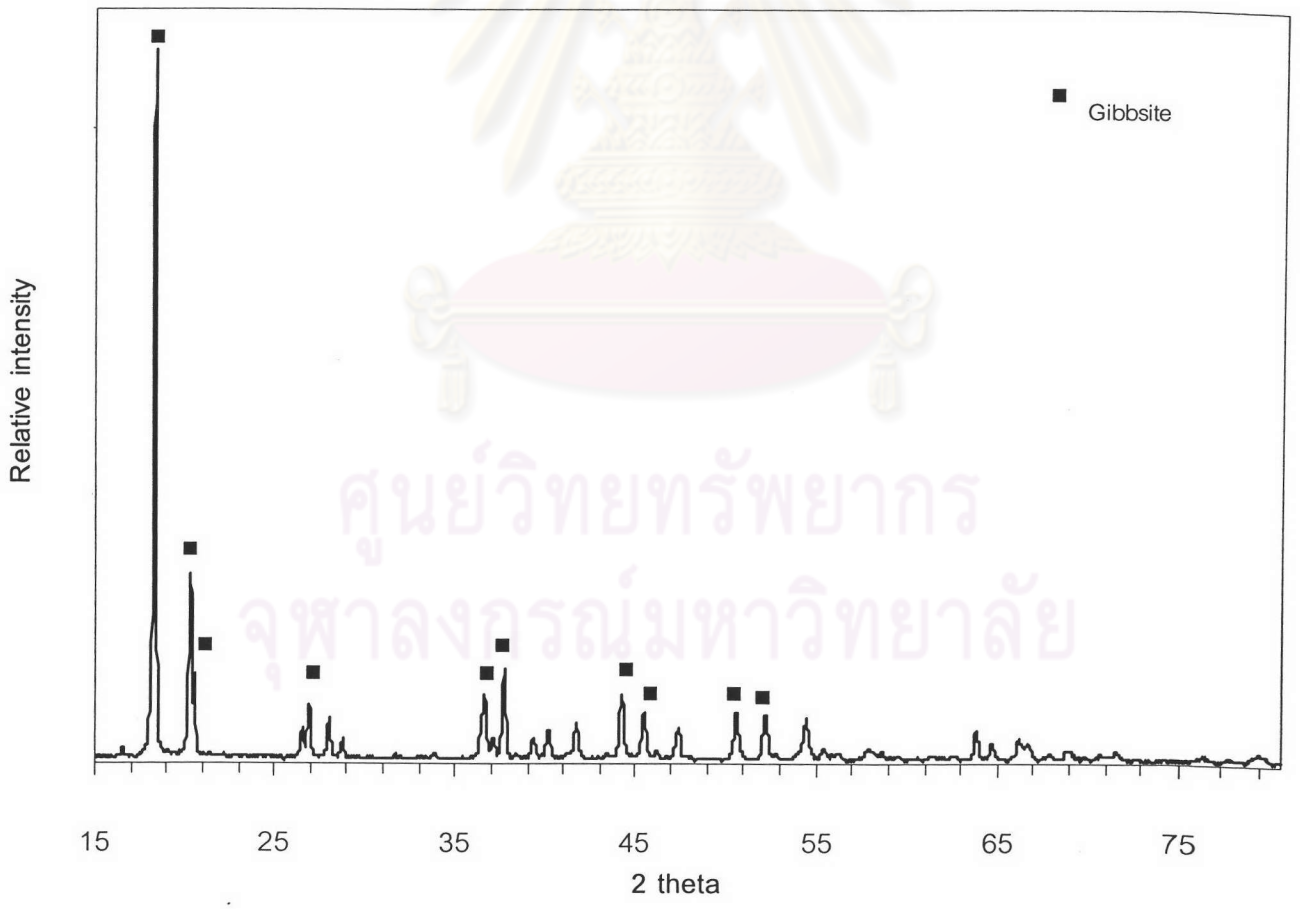

Figure 4.3 XRD pattern of WS.

4.1.3 Microstructures

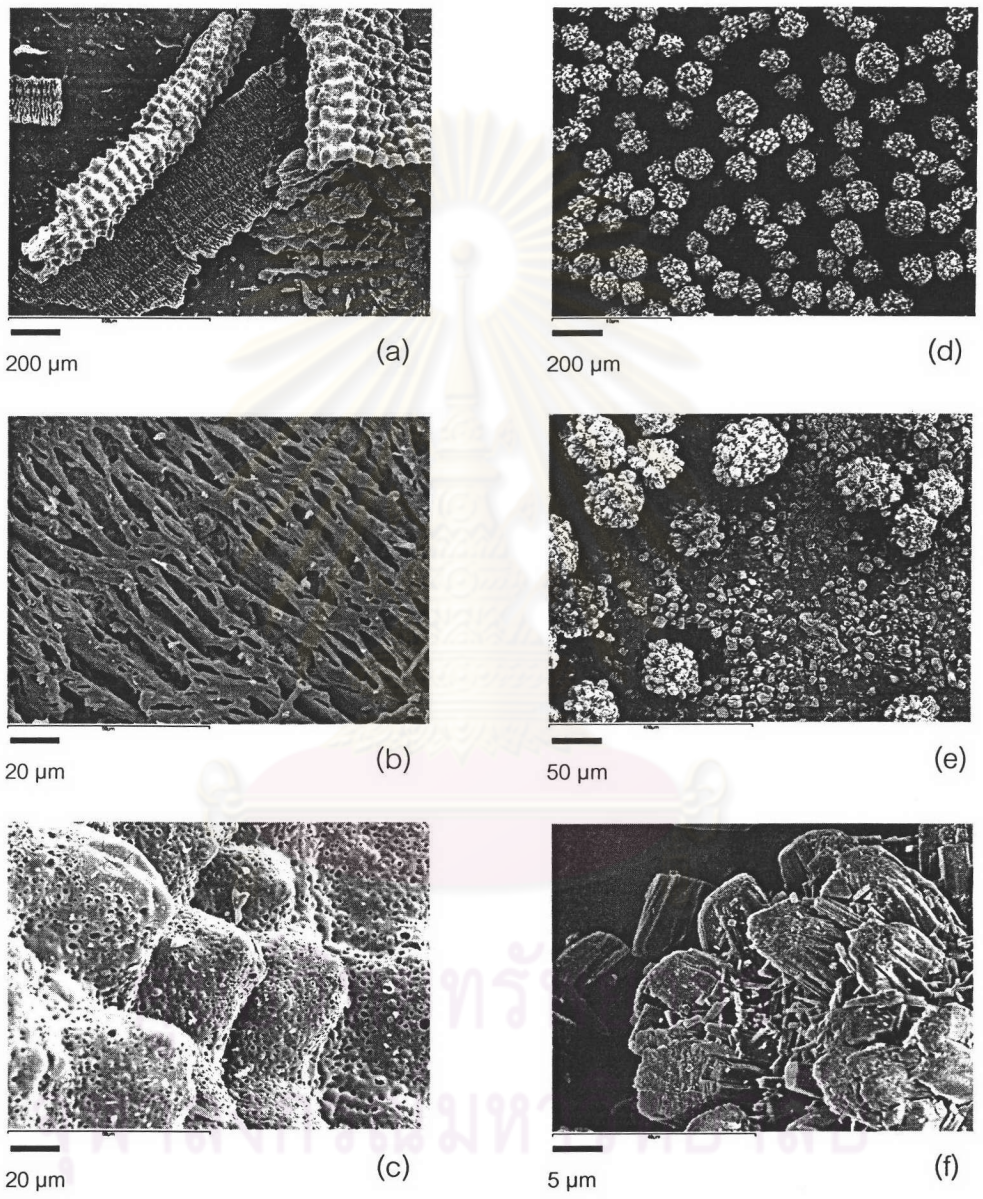

Figure 4.4 SEM micrographs of RHA (a-c) and WS (d-f).

From microstructures of RHA (Figures 4.4 a-c), there are a lot of pores spreading over the inner (b) and outer (c) surfaces. Figures 4.4 d-f show gibbsite crystals clustered loosely. WS powder is rather agglomerate corresponding to the broad particle size distribution observed in Figure 4.1. From these features, it seems not too

difficult to break up and blend the WS agglomerations and the porous grains of RHA in wet milling process.

4.1.4 Thermal analysis

The TGA and correspondent DTA curves of RHA in Figure 4.5 show 1.51% and 3.45% weight loss between 30-185 and 185-500 °C, respectively, indicating the decomposition of moisture content, the structural water and probably residue carbon in RHA. No significant change over the temperature range of 25-1000 °C for SRM30 as shown in Figure 4.6.

Figure 4.5 Thermogravitic Analysis (TGA) and Differential Thermal Analysis (DTA) of RHA.

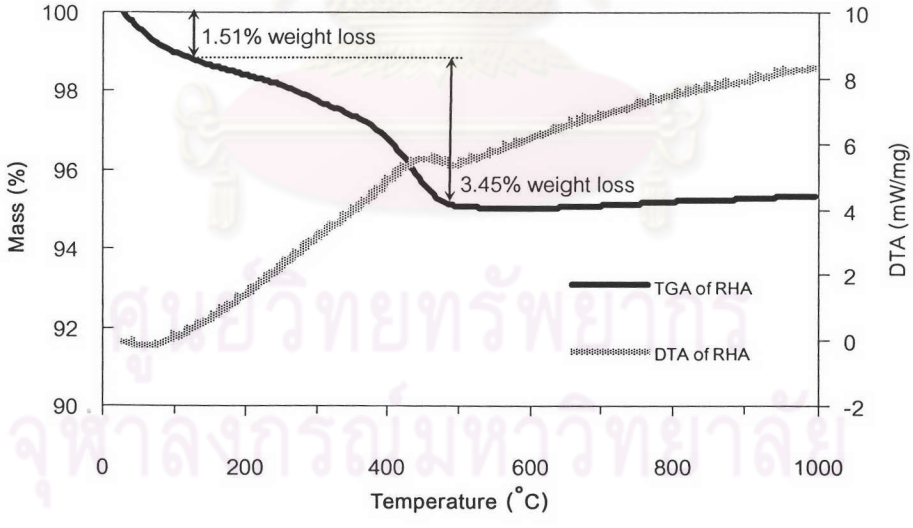

Figure 4.6 Thermogravitic Analysis (TGA) and Differential Thermal Analysis (DTA) of SRM30.

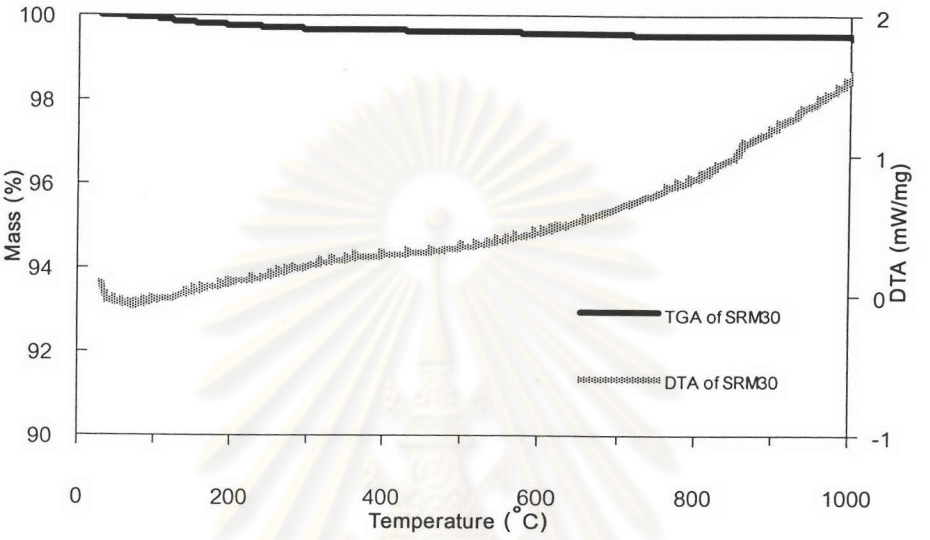

Figure 4.7 Thermogravitic Analysis (TGA) and Differential Thermal Analysis (DTA) of WS.

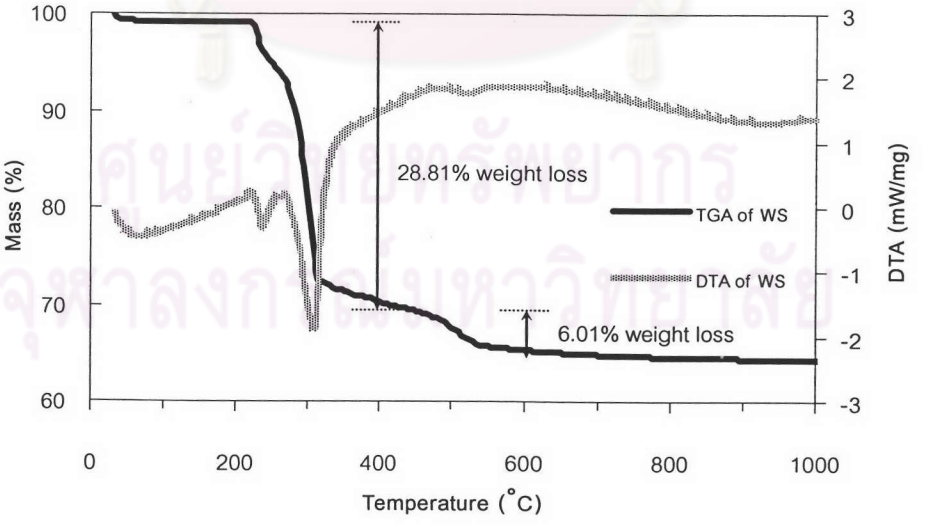

Unlike SRM30, WS shows a remarkable weight loss of 28.81% between 200-400 °C (Figure 4.7, see APPENDIX B for detail) with a correspondent sharp

endothermic DTA peak, due to the hydration of gibbsite ($Al(OH)_3$) structure. The decomposition proceeds slowly at higher temperature, only 6.01% loss is detected. Above 600 °C, the mass change is not significant.

Total loss of WS is ~35%. This figure is large enough to cause a problematic change in dimensions of the body on firing, which leads to cracking. The heat treatment, therefore, must be done carefully during the dehydration temperature.

4.2 Influence of Al_2O_3 Sources on Mullite Formation

SRM30 and WS are used as alumina source for mullite synthesis. Particle size and size distribution of slips are measured as they may influence mullite formation. Phases in the fired specimens were examined by XRD.

4.2.1 Particle Size and Size Distribution of the Solids in the Slips

Under the same preparation conditions, average size and particle size distributions of the solids contents of the slips prepared from two alumina sources are shown in Table 4.4, Figures 4.8 and 4.9. When compare between the slips with the same alumina contents, the slips with SRM30 have smaller solids size than those with WS. SEM micrographs shown in Figure 4.10 tend to show an agreement with the results of size distribution in Figures 4.8 and 4.9.

The size of solids in 60 and 80% SRM30 contents are the finest. It is believed that the alumina powder, which is assumable the hardest among the other precursors, aids milling. The greater its content, the finer the final size is. Between the samples containing WS, the difference in particle size is not apparent and seems not to depend on the amounting of WS.

Table 4.4 Average particle size of RHA/SRM30 and RHA/WS slips milled overnight (24 hours).

slip	80:20A	60:40A	40:60A	20:80A	80:20W	60:40W	40:60W	20:80W
Average particle size	7.28 ±0.01	7.54 ±0.01	2.42 ±0.02	2.17 ±0.01	7.62 ±0.05	6.05 ±0.01	6.03 ±0.04	5.89 ±0.06

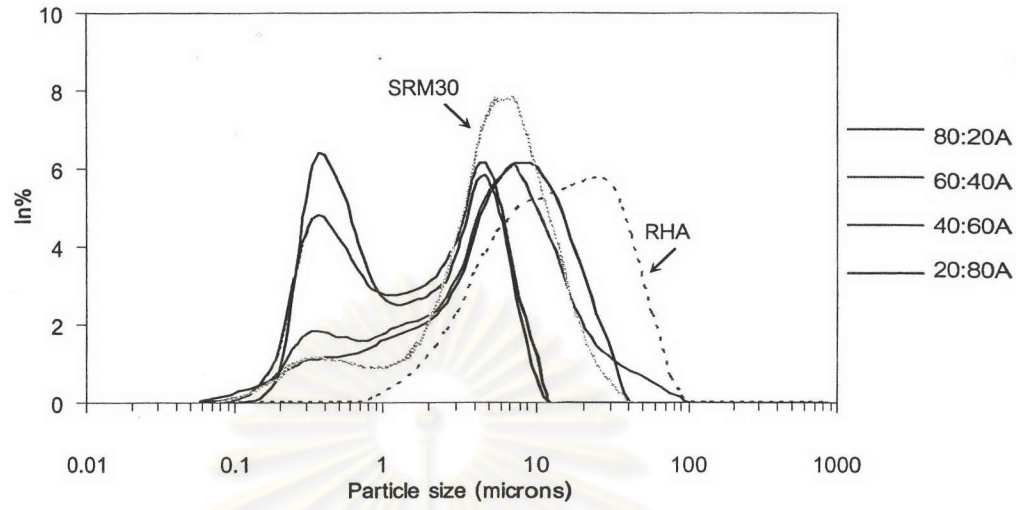

Figure 4.8 Particle size distribution of RHA/SRM30 slips milled overnight (24 hours).

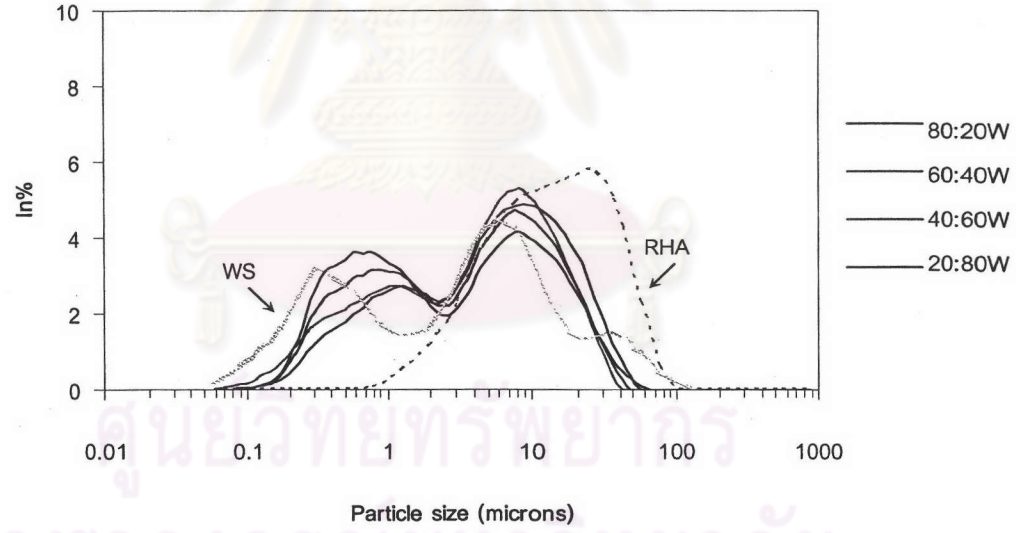

Figure 4.9 Particle size distribution of RHA/WS slips milled overnight (24 hours).

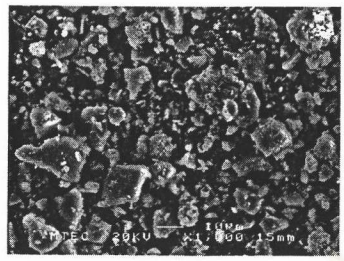

80:20A

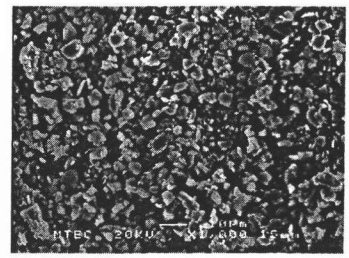

20:80A

80:20W

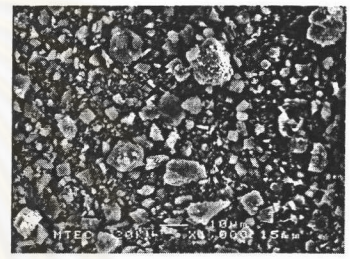

20:80W

Figure 4.10 SEM micrographs of RHA/SRM30 and RHA/WS slips.

4.2.2 Phase Analysis

The bar shaped samples from each slip in the previous section are fired at 1300 °C, 1400 °C and 1500 °C for 2 hours and then XRD examined. For RHA/SRM30 samples, peaks of mullite are detectable at 1500 °C (Figure 4.13), below this temperature (Figure 4.11 and 4.12) only SiO_2 in cristobalite form and Al_2O_3 are observed.

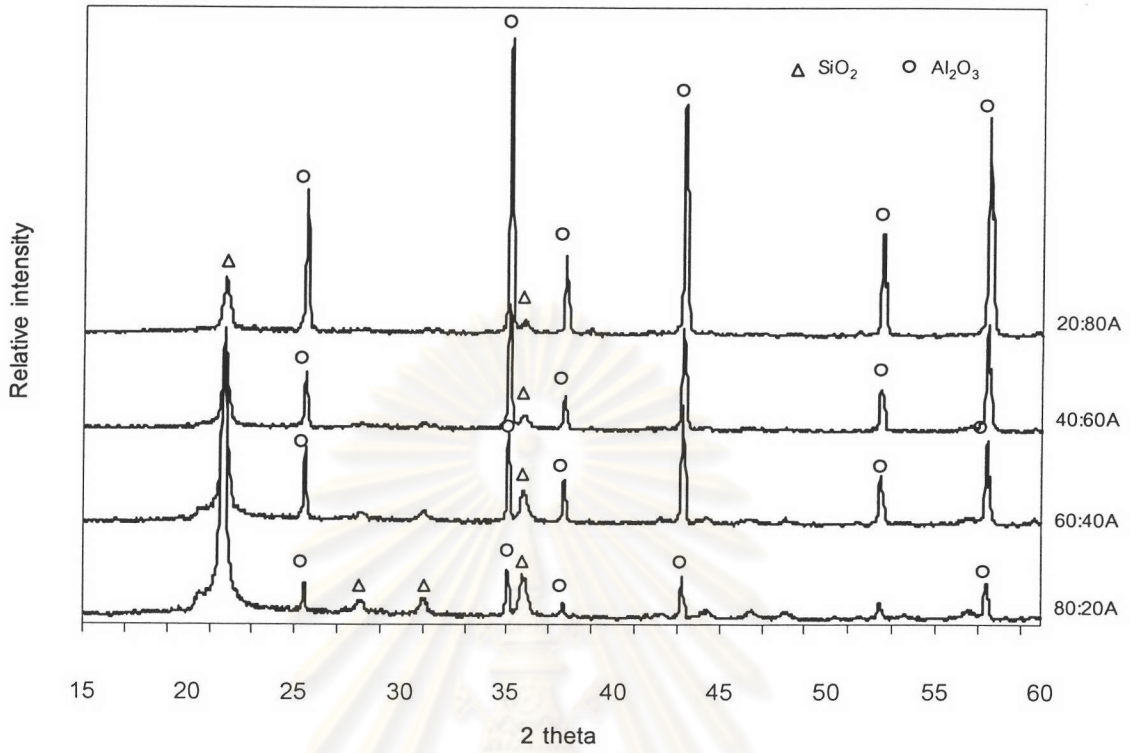

Figure 4.11 XRD patterns of RHA/SRM30 specimens fired at 1300 °C for 2 hours.

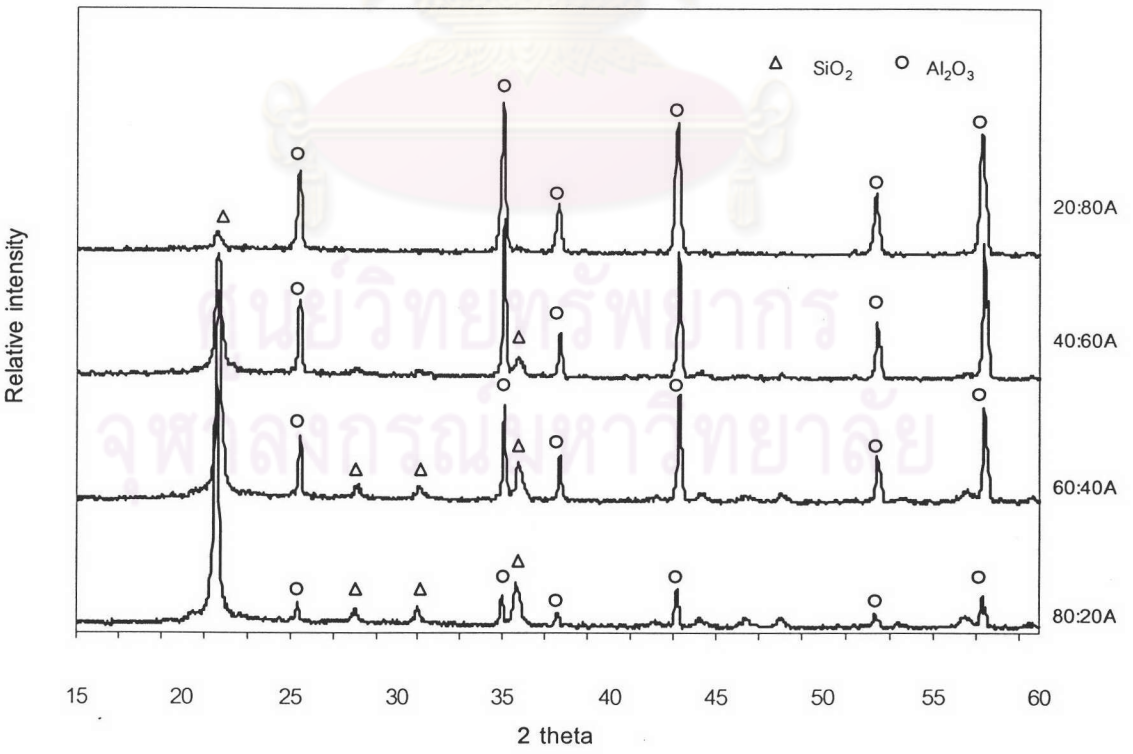

Figure 4.12 XRD patterns of RHA/SRM30 specimens fired at 1400 °C for 2 hours.

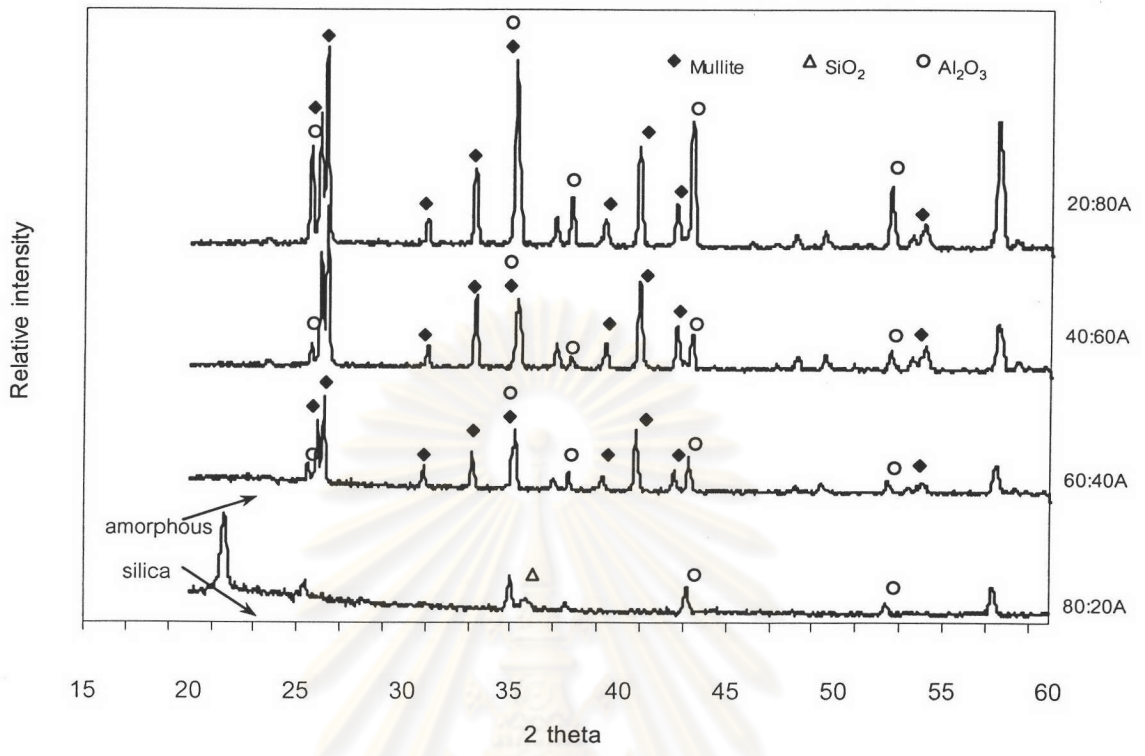

Figure 4.13 XRD patterns of RHA/SRM30 specimens fired at 1500 °C for 2 hours.

Stoichiometric mullite consists of $3Al_2O_3$ and $2SiO_2$. Therefore, 71.83wt% of Al_2O_3 and 28.17wt% of SiO_2 are needed for complete mullitization. RHA-S/SRM30 samples have the compositions shown in Tables 4.5, which Al_2O_3 and SiO_2 are partly taken or used up to form mullite (See APPENDIX C for details). However, mullite is not detectable until 1500 °C (Figures 4.11-4.13). It is evident that mullitization of RHA-S/SRM30 samples at this temperature is not yet completed. Figure 4.13 shows the remained of Al_2O_3 and SiO_2 in the most of samples. The mullitization may be hindered by less reactivity of the Al_2O_3 powder.

Table 4.5 Estimate of composition of the RHA/SRM30 samples.

slips	Before mullitization		After mullitization				
	Al_2O_3	SiO_2	Mullite	Al_2O_3		SiO_2	
				used	remain	used	remain
80:20A	20.00	77.66	27.84	20	0.00	7.84	69.82
60:40A	40.00	58.25	55.69	40	0.00	15.69	42.56
40:60A	60.00	38.83	83.53	60	0.00	23.53	15.30
20:80A	80.00	19.42	68.93	49.51	30.49	19.42	0.00

While for RHA/WS samples, mullite formation is found at from 1300 °C onwards (Figures 4.14 and 4.15). This is inconsistency with work done by Okada, K. [32], which is suggested that mullitization temperatures change according to the particle sizes of the starting materials but are not lower than 1200 °C.

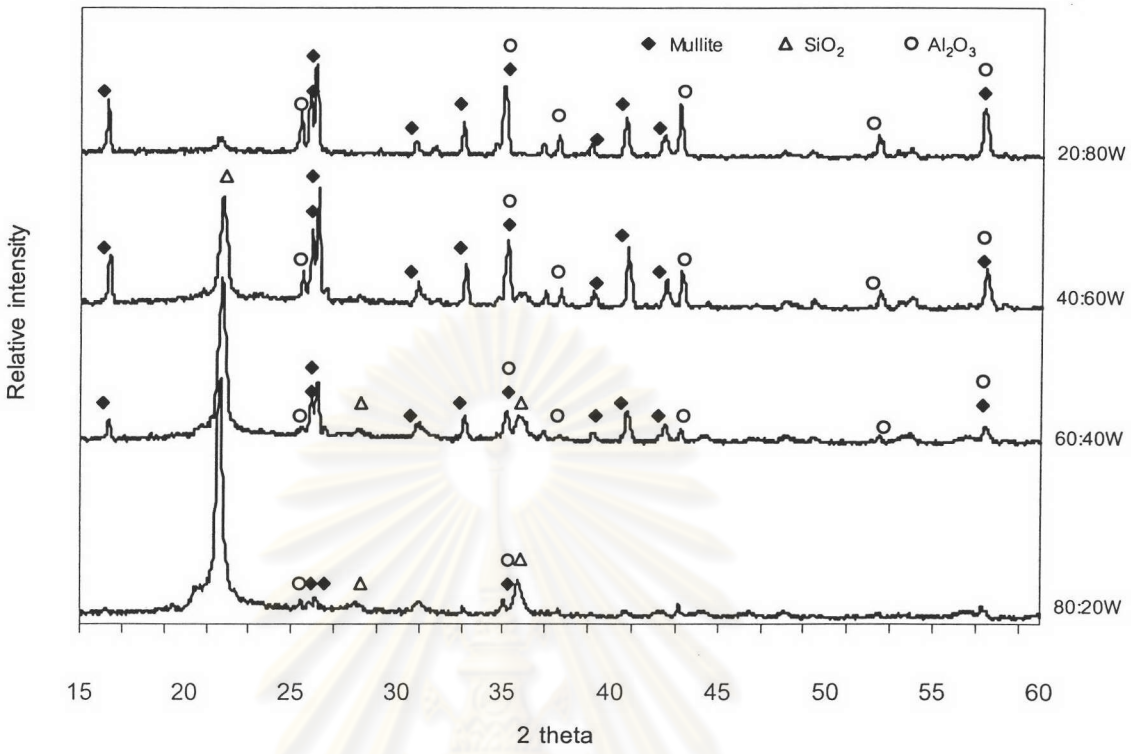

Figure 4.14 XRD patterns of RHA/WS specimens fired at 1300 °C for 2 hours.

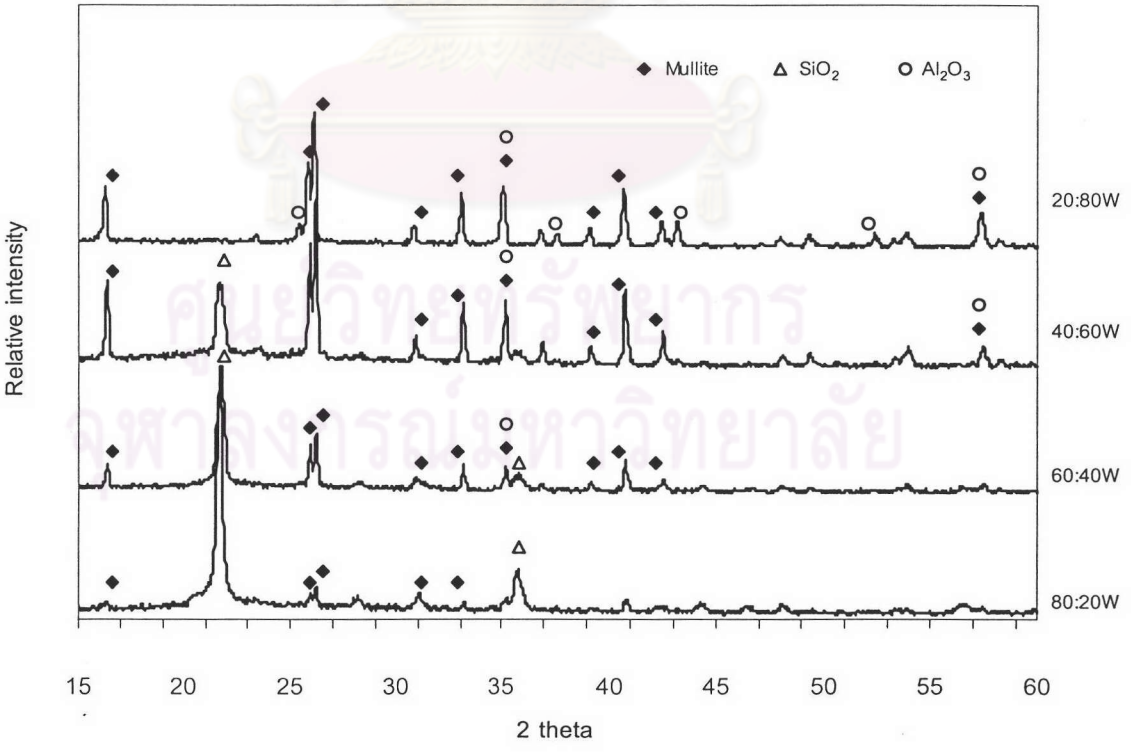

Figure 4.15 XRD patterns of RHA/WS specimens fired at 1400 °C for 2 hours.

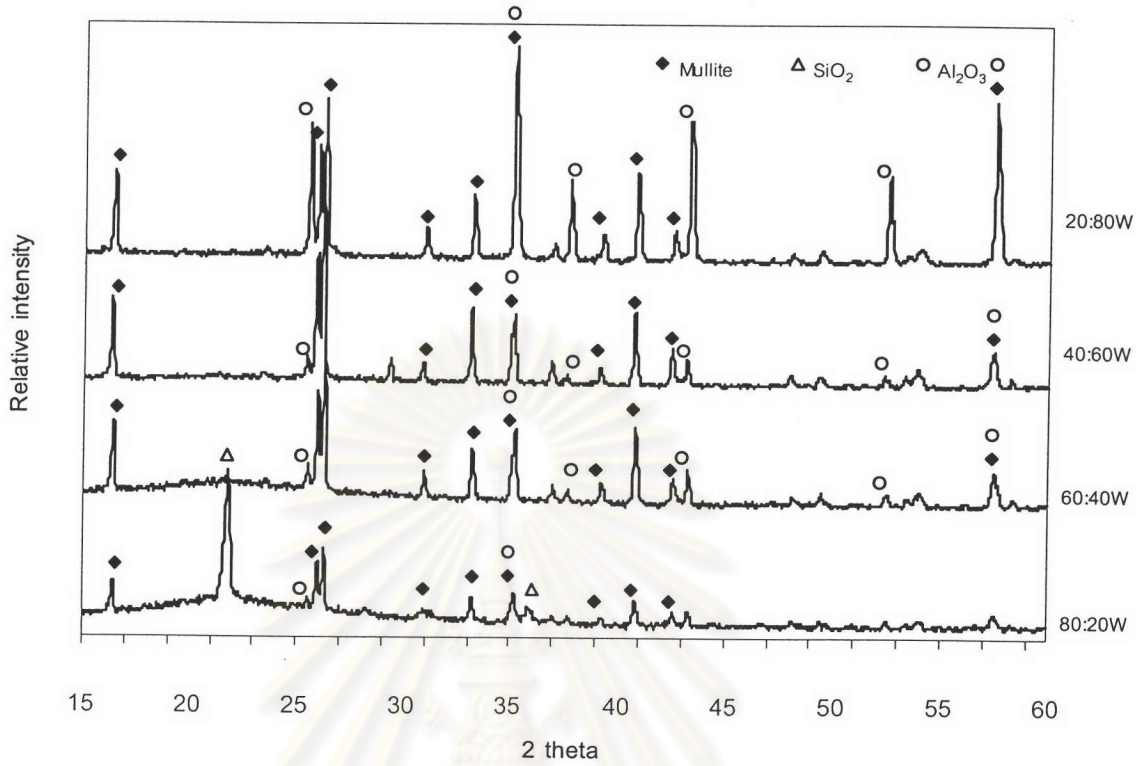

Figure 4.16 XRD patterns of RHA/WS specimens fired at 1500 °C for 2 hours.

From the calculation (Table 4.6-see APPENDIX C for detail), 20.6 wt% RHA and 79.4 wt% WS give the stoichiometric mullite. However, both precursors are still remained to some degree at 1300 °C, but not as much as in RHA/SRM30 samples. Higher energy or higher temperature is required to complete the reaction (see section 4.4.3.1).

Table 4.6 Composition estimate in the RHA/WS samples.

slips	Before mullitization		After mullitization				
	Al_2O_3	SiO_2	Mullite	Al_2O_3		SiO_2	
				used	remain	used	remain
80:20W	12.86	77.66	17.91	12.86	0.00	5.04	72.62
60:40W	25.72	58.25	35.81	25.72	0.00	10.09	48.16
40:60W	38.59	38.83	53.72	38.59	0.00	15.13	23.70
20:80W	51.45	19.42	68.93	49.51	1.94	19.42	0.00

Although RHA/SRM30 slips have particle sizes smaller than RHA/WS samples (Table 4.4), the mullitization temperature of RHA/SRM30 samples is higher than RHA/WS. It is assumed that WS is more activated as it has higher surface area which is resulted from the decomposition of structural water before the mullitization commences.

WS is cheaper waste and more effective on mullitization than SRM30. Therefore, it is chosen for the next investigation.

4.3 Effect of Deflocculant Amount on Rheology

DarvanC is added from 0.1-0.5% into each slip. The slips are then brought to measure the viscosity using shear rate ranges from 10-200 rpm to establish the relationship of rheological properties such that the appropriate amount of DarvanC is known.

The plots of shear stress vs shear rate for 40:60WS_H, 30:70WS_H and 20:80WS_H are manifested in Figures 4.17-4.22.

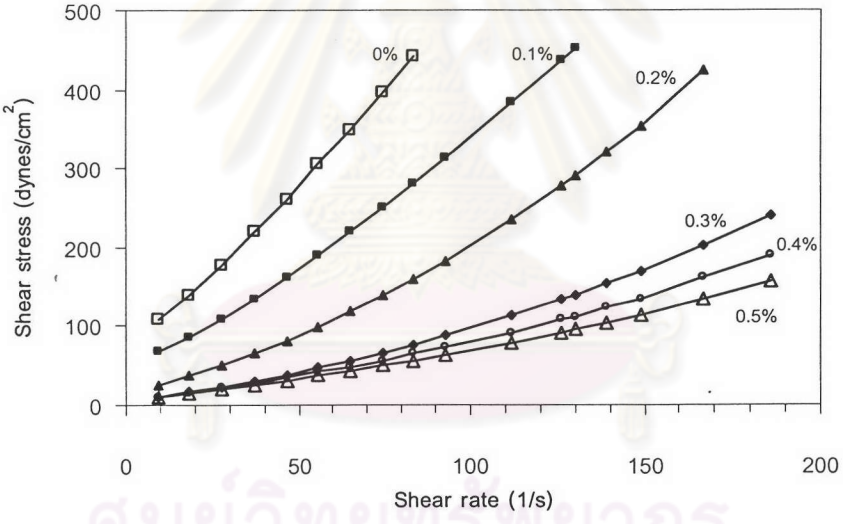

Figure 4.17 Shear stress and shear rate of RHA:WS_H=40:60 slip with various %DarvanC, milled overnight (24 hours).

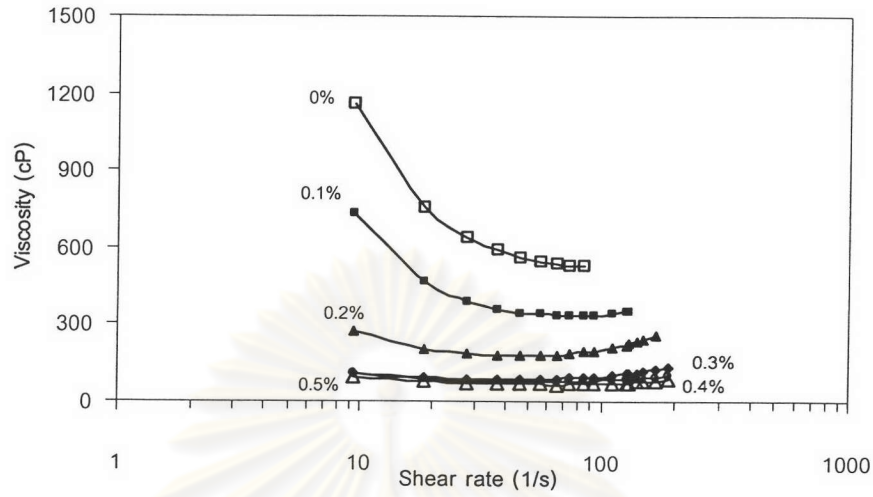

Figure 4.18 Viscosity and shear rate of RHA:WS_H=40:60 slip with various %DarvanC, milled overnight (24 hours).

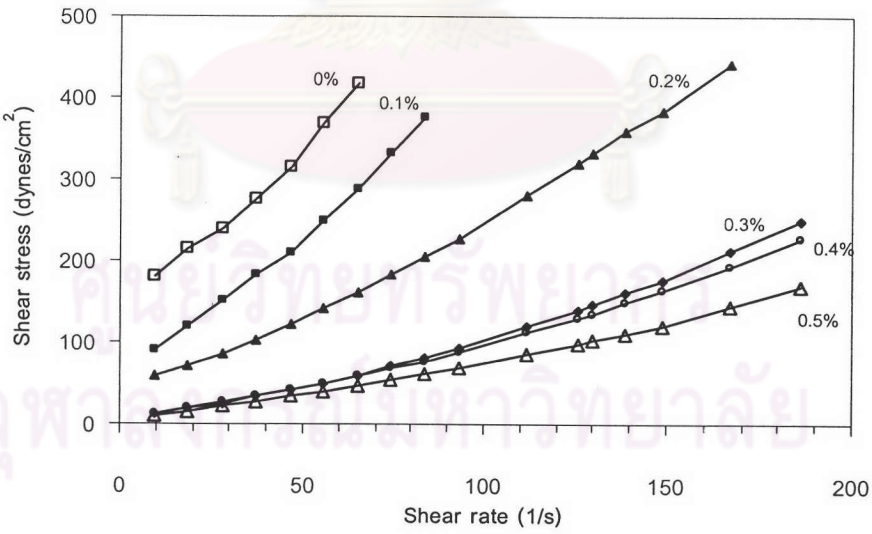

Figure 4.19 Shear stress and shear rate of RHA:WS_H=30:70 slip with various %DarvanC, milled overnight (24 hours).

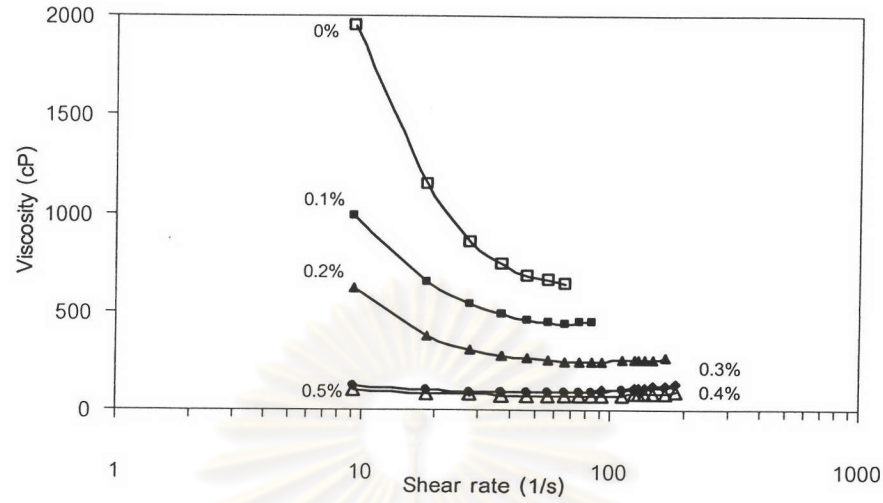

Figure 4.20 Viscosity and shear rate of RHA:WS_H=30:70 slip with various %DarvanC, milled overnight (24 hours).

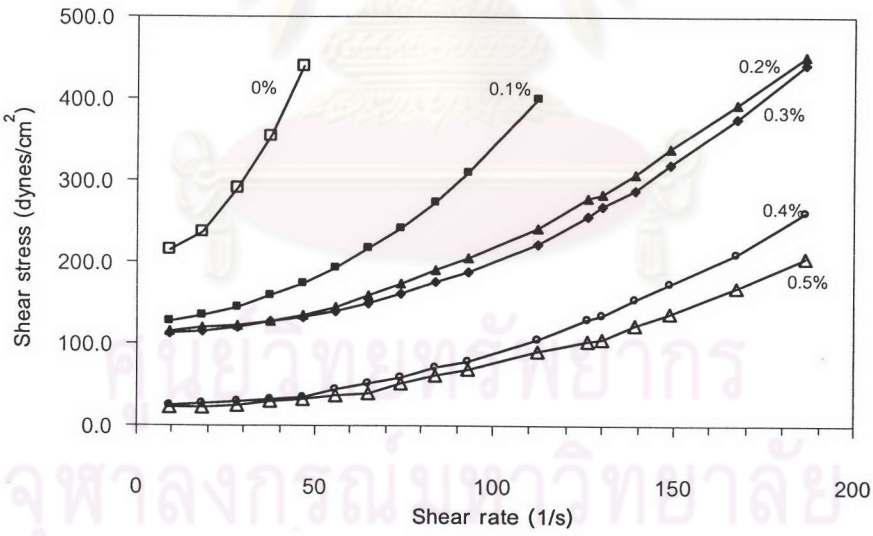

Figure 4.21 Shear stress and shear rate of RHA:WS_H=20:80 slip with various %DarvanC addition, milled overnight (24 hours).

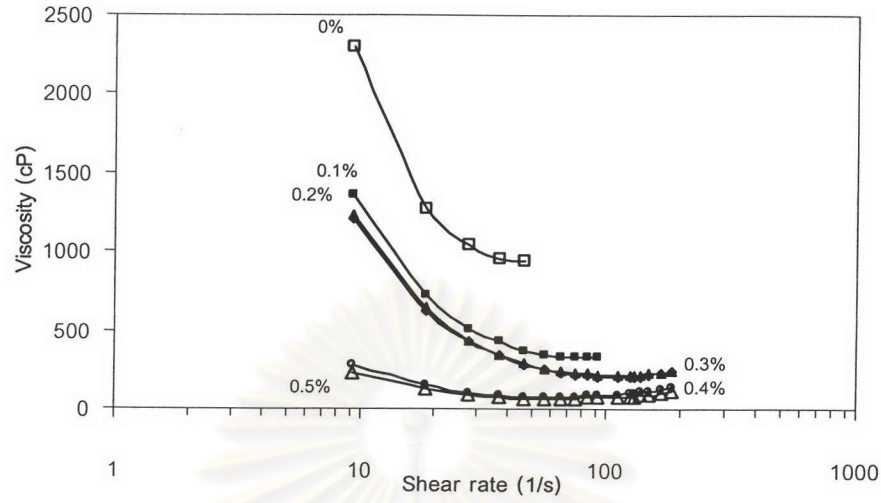

Figure 4.22 Viscosity and shear rate of RHA:WS_H=20:80 slip with various %DarvanC, milled overnight (24 hours).

The slips of all compositions under this study exhibit shear thinning or pseudoplastic behavior, the viscosity decreases with increasing in shear rate (Figures 4.18, 4.20 and 4.22). This rheological behavior is preferable for industrial processing. This means the slip adjusted is be well-mixed, easily pumped and poured filling mold. The viscosity, which is a slope of a plot between shear stress and shear rate, declines as the amount of DarvanC increases (Figures 4.17, 4.19 and 4.21). The amount of DarvanC that gives the viscosity independent on shear rate is 0.3, 0.3 and 0.4% for RHA:WS = 40:60, 30:70 and 20:80 is, respectively.

4.4 Effect of Size of Solids Content on Properties of the Final Product.

4.4.1 Particle Size and Size Distribution

The particle size distribution of 4L, 3L, 2L and 4S, 3S, 2S are much dependent on milling time rather than WS_H content (Figure 4.23 and Table 4.7). For RHA/WS_H system, it is found that too large particle size > 7-8 μm causes difficulty in mold removal, whereas too small size < 2.5-3 μm causes too much shrinkage before the casting finishes.

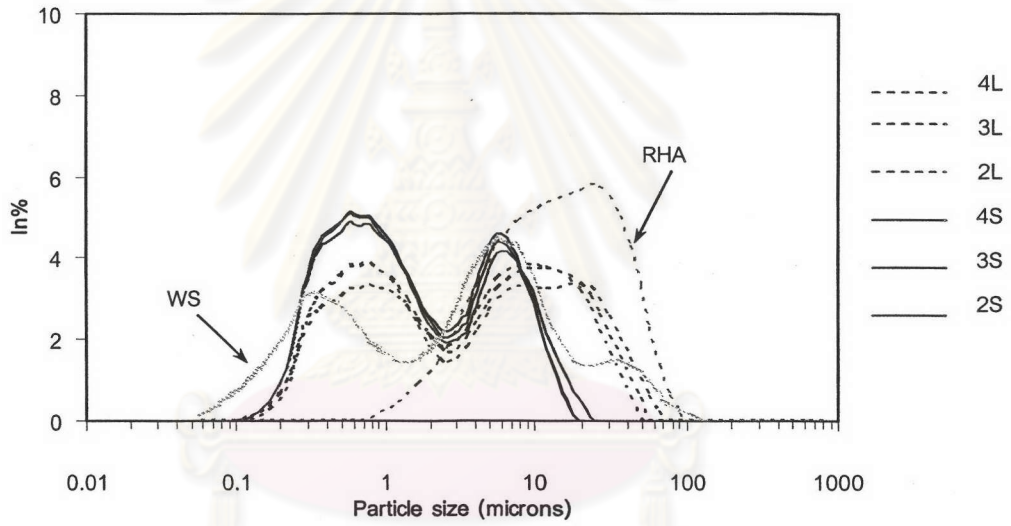

Figure 4.23 Particle size distribution of RHA/WS_H slips milling time 13 hrs (4L, 3L, 2L) and 48 hrs (4S, 3S, 2S).

Table 4.7 Average particles size of solids in the slips.

Slips	4L	3L	2L	4S	3S	2S
Avr. Particle size (μm)	7.33 ±0.05	6.44 ±0.13	8.17 ±0.04	2.77 ±0.01	2.72 ±0.02	2.98 ±0.02

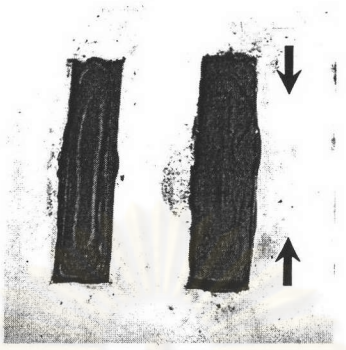

Figure 4.24 The specimens were fabricated from slips containing too large particles (left) and right size particles (right).

4.4.2 Densities of Slip

The densities of 4L, 4S, 3L, 3S, 2L and 2S are shown in Table 4.8, the value ranges from 1.56-1.60 g/cm^3. The values of 2L and 2S are slightly higher than these of 3L, 3S, 4L, and 4S because they contain more WS which has higher density than RHA (densities of RHA and WS are 2.18 and 2.60, respectively).

Table 4.8 Densities of RHA/WS_H slips.

Slip	4L	3L	2L	4S	3S	2S
Density (g/cm^3)	1.56 ±0.01	1.58 ±0.01	1.60 ±0.01	1.56 ±0.01	1.58 ±0.01	1.60 ±0.01

4.4.3 Characterizations of the Fired Specimens

4.4.3.1 Composition and Phase Analysis

Oxide contents from the XRF analysis and the calculation derived from thermal analysis of each sample are shown in Table 4.9 (see APPENDIX D for detail). The result is in consistency with the calculation. Using the figures from Table 4.9, %mullite, Al_2O_3 and SiO_2 residues in the fired bodies can be estimated (see Table 4.10). 25.93% RHA and 74.06% WS_H give the stoichiometric mullite.

Table 4.9 Sample compositions in specimens from XRF and calculation.

Sample	Compositions			
	From XRF		From calculation	
	% Al_2O_3	%SiO_2	% Al_2O_3*	%SiO_2*
4L	55.03	41.64	57.26	42.74
4S	55.43	41.40		
3L	65.59	31.58	67.57	32.43
3S	65.41	31.78		
2L	76.38	21.45	78.13	21.87
2S	76.08	21.54		

* % Al_2O_3 and %SiO_2 are calculated from thermal analysis and XRF, respectively.

Table 4.10 Estimate of phase contents, using the data from XRF analysis.

Samples	Phases				
	%Mullite	$\%Al_2O_3$		$\%SiO_2$	
		used	remained	used	remained
4L	76.61	55.03	0	21.58	20.06
4S	77.17	55.43	0	21.74	19.66
3L	91.31	65.59	0	25.72	5.86
3S	91.06	65.41	0	25.65	6.13
2L	76.15	54.70	21.68	21.45	0
2S	76.47	54.93	21.15	21.54	0

All of the samples are fired at 1400 °C and subsequently at 1700 °C. XRD patterns in Figures 4.25 and 4.28 show the presence of silica residue in 4L and 4S samples in amorphous form (hump at ~20° 2 theta). At 1400 °C, the Al_2O_3 peaks are observed in 4L and 3L samples (Figure 4.25) and disappear after the samples are fired at 1700 °C (Figure 4.26). Unlike 4S and 3S samples, the alumina peaks are not noticeable since after 1400 °C heating (Figure 4.27). It is believed that the particle size of solids plays a role in mullitization; smaller particle size gives higher surface area and thus higher reaction rate.

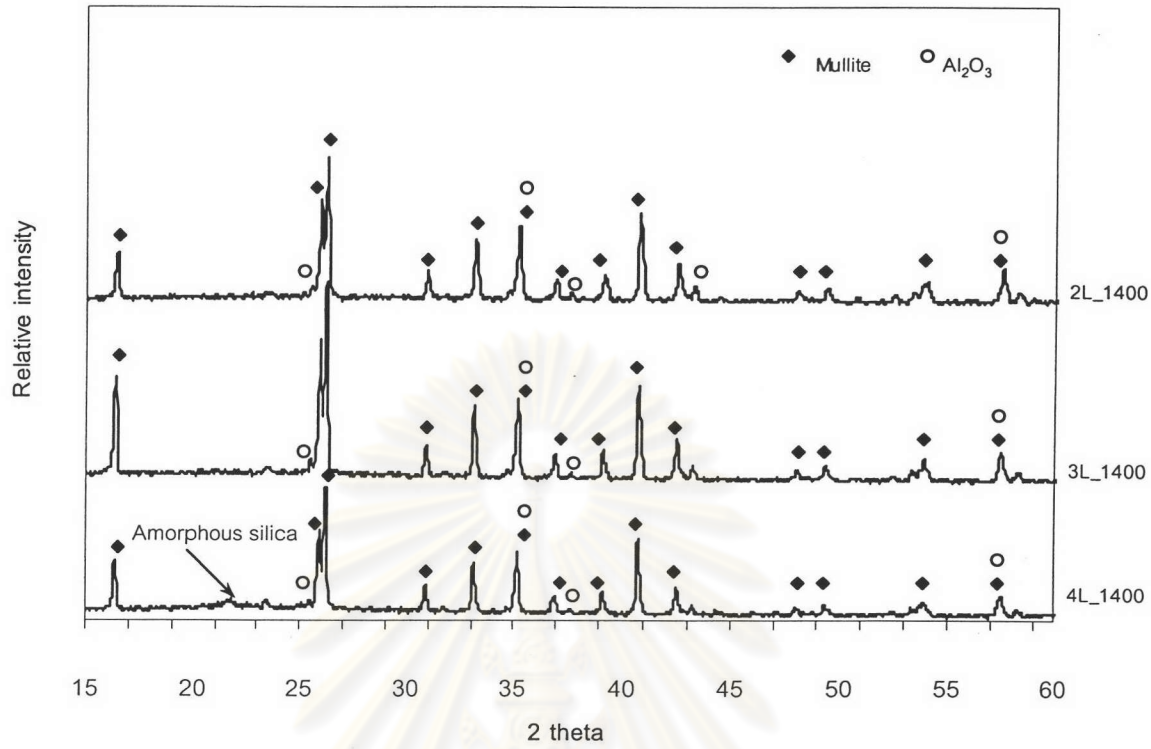

Figure 4.25 XRD patterns of 4L, 3L and 2L specimens fired at 1400 °C for 2 hours

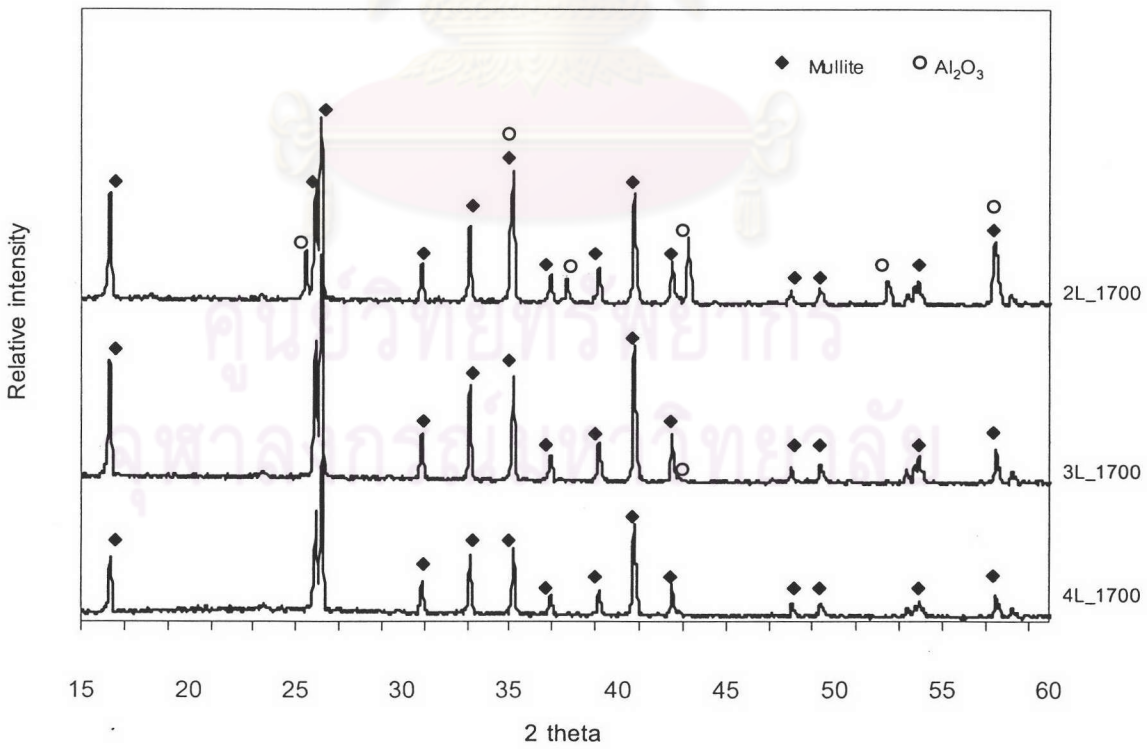

Figure 4.26 XRD patterns of 4L, 3L and 2L specimens fired at 1700 °C for 1 hour.

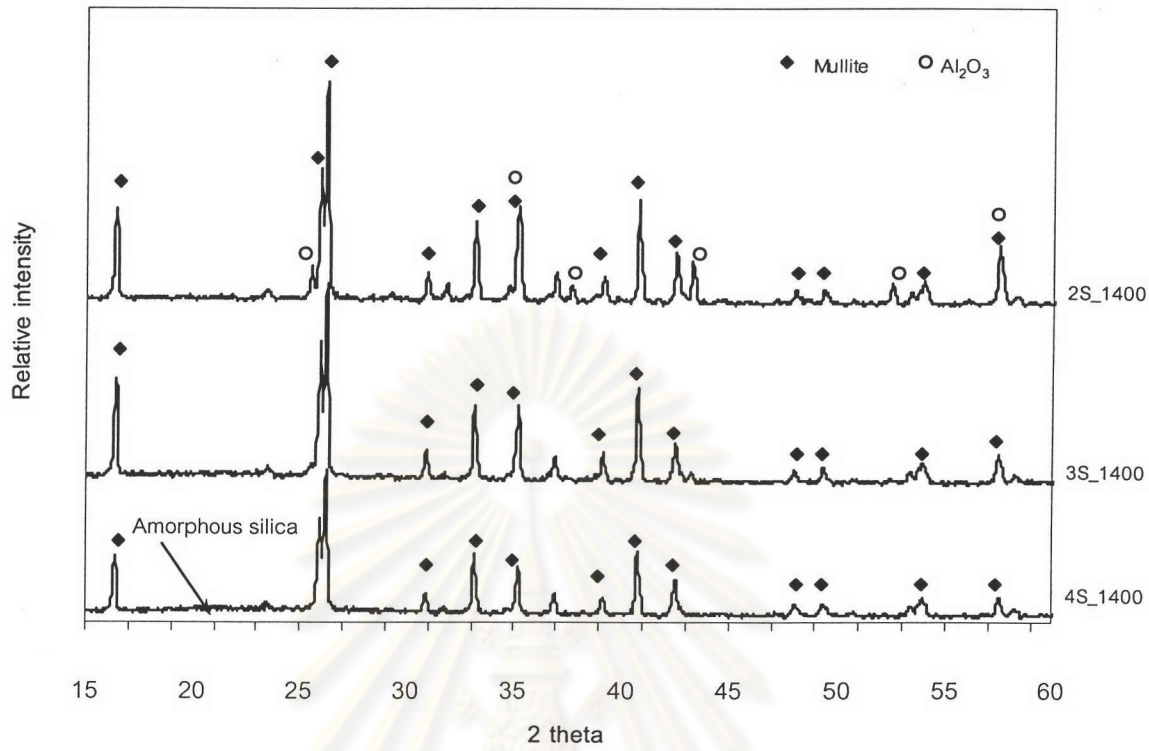

Figure 4.27 XRD patterns of 4S, 3S and 2S specimens fired at 1400 °C for 2 hours.

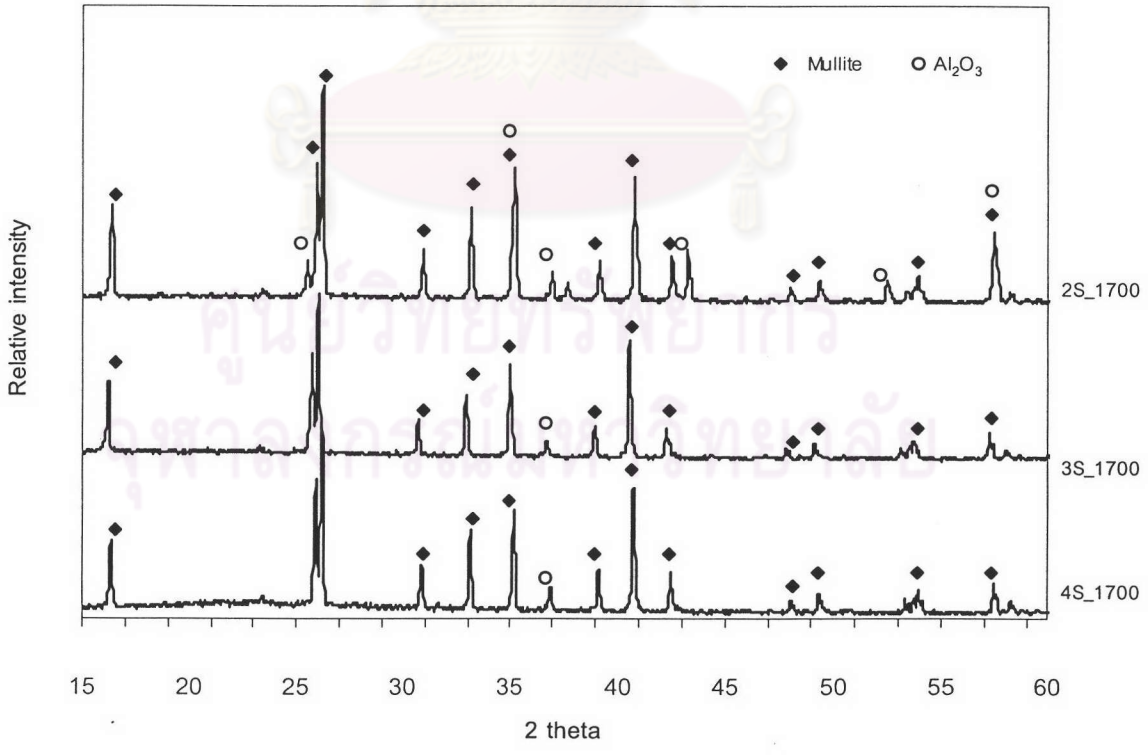

Figure 4.28 XRD patterns of 4S, 3S and 2S specimens fired at 1700 °C for 1 hour.

4.4.3.2 Microstructure

Etched surfaces of the samples are shown in Figure 4.29. SEM micrographs (a) and (b) represent voids where the residual glass used to be. From the estimate of phase contents (Table 4.10), 4S and 3S contain ~20 and 6 wt% excessive silica, respectively. High aspect ratio mullite grains are found intensively in all specimens. The grains are generally 3 μm in width and 10 μm in length. In 2S sample, mullite grains are found with polygonal grains of residual Al_2O_3.

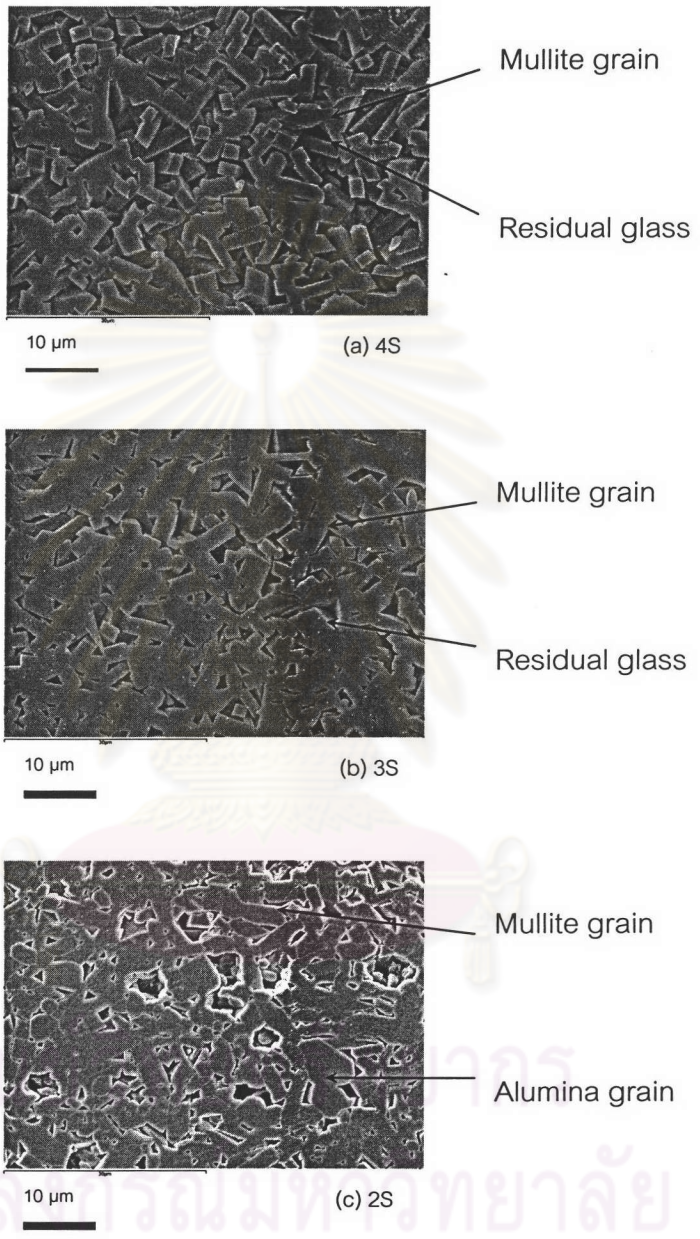

Figure 4.29 SEM micrographs of specimens fired at 1700 °C.

4.4.3.3 Physical Properties

After heat treatment, all samples shrink and become denser, presumably the specimens undergo sintering and mullitization simultaneously. These incidents lead to physical changes in density, % apparent porosity and % water absorption.

At 1400 °C, the shrinkage of the 4S sample is exhibits a highest and its resultant density is 1.95 g/cm^3. (Figures 4.30 and 4.31 (a)). Starting RHA contains high silica noticeably and other impurity oxides. It is explained that the presence of impurities enhances early softening and melting of silica leading to a large decrease in volume. Generally, the softening of silica occurs around 600-900 °C [47].

Not only the silica content, but also the particle size greatly affects the density of samples. Sintering temperature is inversely proportional to r, where r is the particle size [42]. Therefore, 2S, 3S and 4S are more densified than the 2L, 3L and 4L. The correspondent apparent porosity and %water absorption, which represent the volume of open pores, have opposite trends to the density. At 1400 °C, the sintering is not yet completed, the body contains more pores and has high % water absorption (Figures 4.31 (b) and (c)).

Further heat treatment to 1700 °C leads to more shrinkage and higher density. The % apparent porosity and % water absorption decrease apparently (Figures 4.31 (b) and 4.31 (c)). The % volume of firing shrinkage, density, %apparent porosity and %water absorption of 4S are not different from those of 4L, regardless of particle size. At this temperature, 4S and 4L, which have more silica readily to melt to fill pores, become higher in density. Whereas, the others with lower RHA contents have these properties dependent on both RHA content and particle size, as found for 1400 °C fired samples.

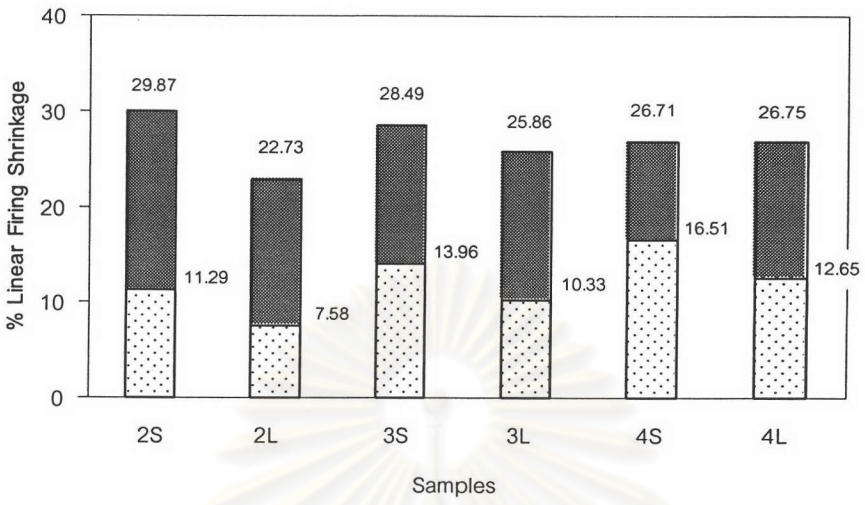

Figure 4.30 Percent linear firing of shrinkage of the specimens fired at 1400 (dotted) and 1700 °C (shaded).

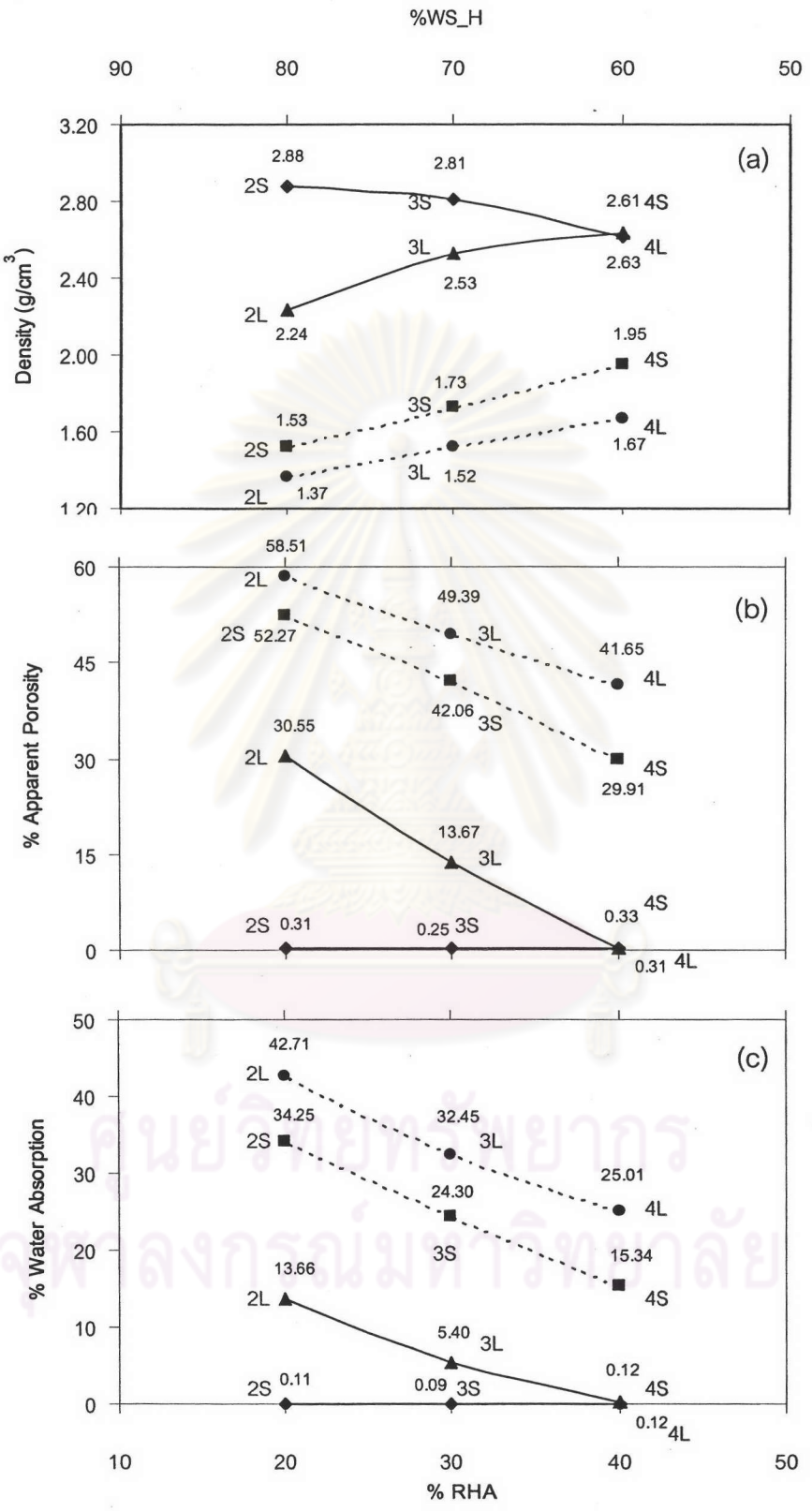

Figure 4.31 Density, Apparent porosity and Percent water absorption after firing at 1400 (dotted line) and 1700 °C (solid line).

The bulk densities of the small samples are lower than the theoretical value (densities of mullite=3.2 g/cm^3 and alumina=3.98 g/cm^3). However, the volume of open porosity, i.e. %apparent porosity, is far below 1%. Therefore, there might have been closed pores in the structure. Figure 4.32 shows the optical microscopic observation of the sectioned specimens. Figure 4.33 depicts the corresponding %porosity from the image analysis. The pores seen in this picture include the open and closed pores in the structure.

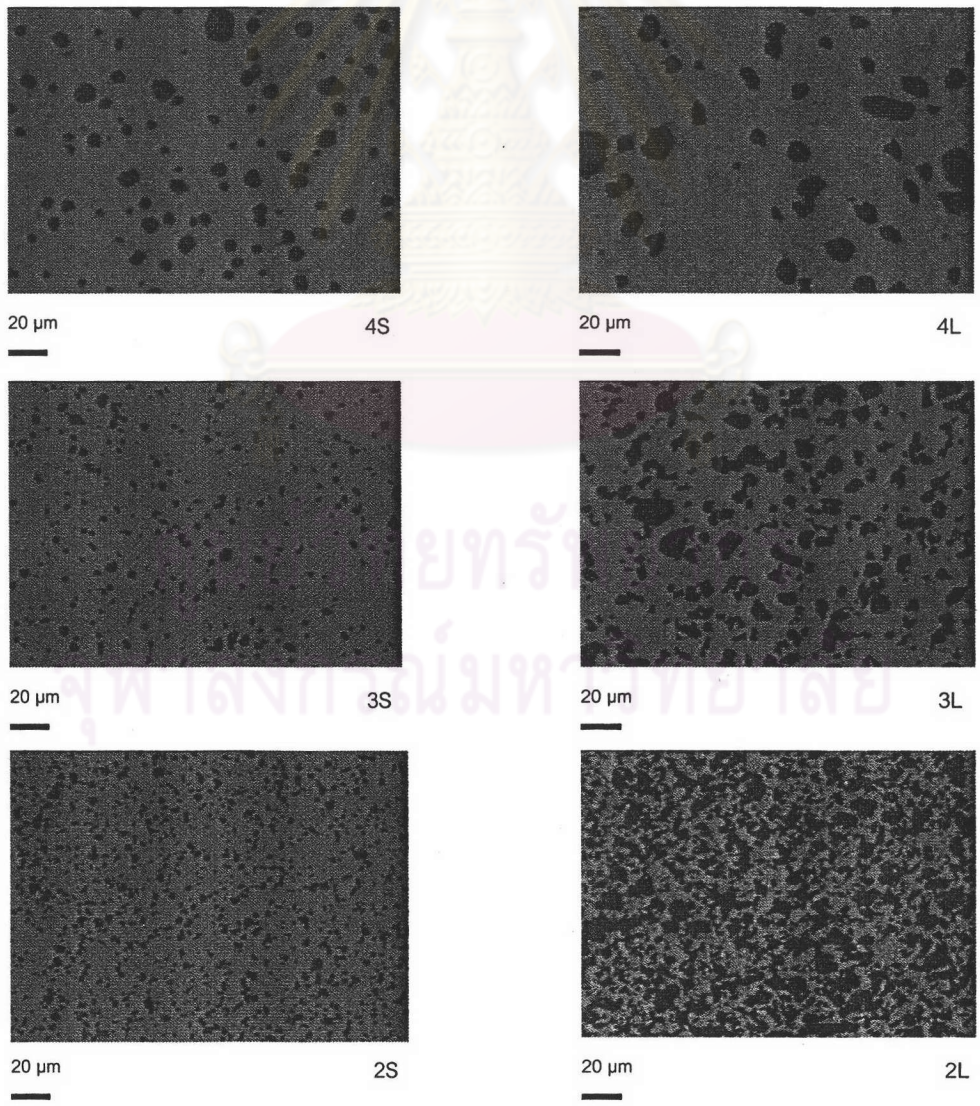

Figure 4.32 Optical microscopic observation of the specimens fired at 1700 °C.

From Figures 4.32, the pores are found most intensively in the sample has high WS_H content. Large size pores occur in the sample produced from large size precursors, compare 4S with 4L, 3S with 3L and 2S with 2L.

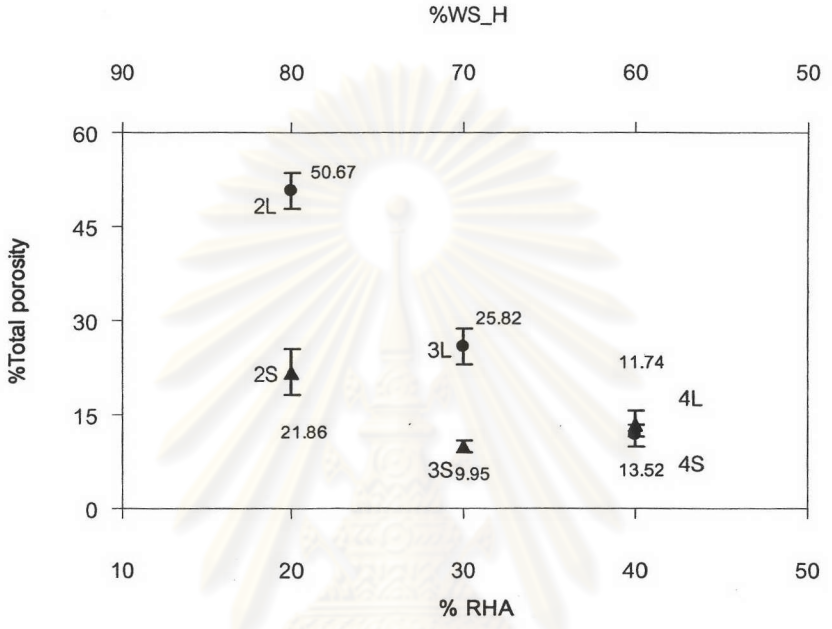

Figure 4.33 % Porosity of specimens fired at 1700 °C by image analysis.

Total porosity in all samples is thought to arise from

1) encapsulated carbon in RHA,

2) thermal decomposition of the WS_H,

3) not enough silica to fill the pores,

4) incomplete sintering and

5) poor particle packing.

The larger RHA particles have more carbon encapsulated. As the temperature rises and before the sintering commences, only carbon on the surface of the particles is burn out. The encapsulated carbon is presumably oxidized during or after the sintering. Bubbles from the oxidation generate pores in the body. Therefore, the higher amount of the coarse particles, the more pores are found. While for smaller particle, carbon tends to present at the surface and the bubbles formed can escape

more easily and probably before the sintering begins, leaving smaller pores in the structure.

Whereas, high %WS_H samples have more structural water. When it is heat from 250-600 °C, the water leaves the structure and more micropores are expectedly present all over the body. Up to 1700 °C, the sintering is still not yet completed and silica is used up for mullitization. Consequently, the voids are left throughout the body. Despite silica is excessive, the sintering in 4L, 4S, 3L and 3S is still not completed. Micropores are still seen spreading over. Apart from the problem of encapsulated carbon, it is believed that grains of mullite, which grow in random directions, obstruct the flow of glassy phase and the densification is hindered.

The particle size of the precursor also has an effect on porosity, particularly in the sample having low RHA content. The samples made from the smaller particles contain less pores and have higher density. This is because of better packing of the small particles and voids are relatively small. Dense particle packing shortens diffusion paths and hence accelerates sintering. The best densification or least porosity is therefore found for the 3S sample which has excessive silica and good particle packing.

4.4.3.4 Mechanical Properties

In the samples derived from small size precursors, the modulus does not show a trend with % porosity (Figure 4.34) but the % RHA or glass content. In contrast, the samples made from large precursors are likely to have a decreasing trend with % porosity. However, more data needed to clarify the effects of glass content and % porosity.

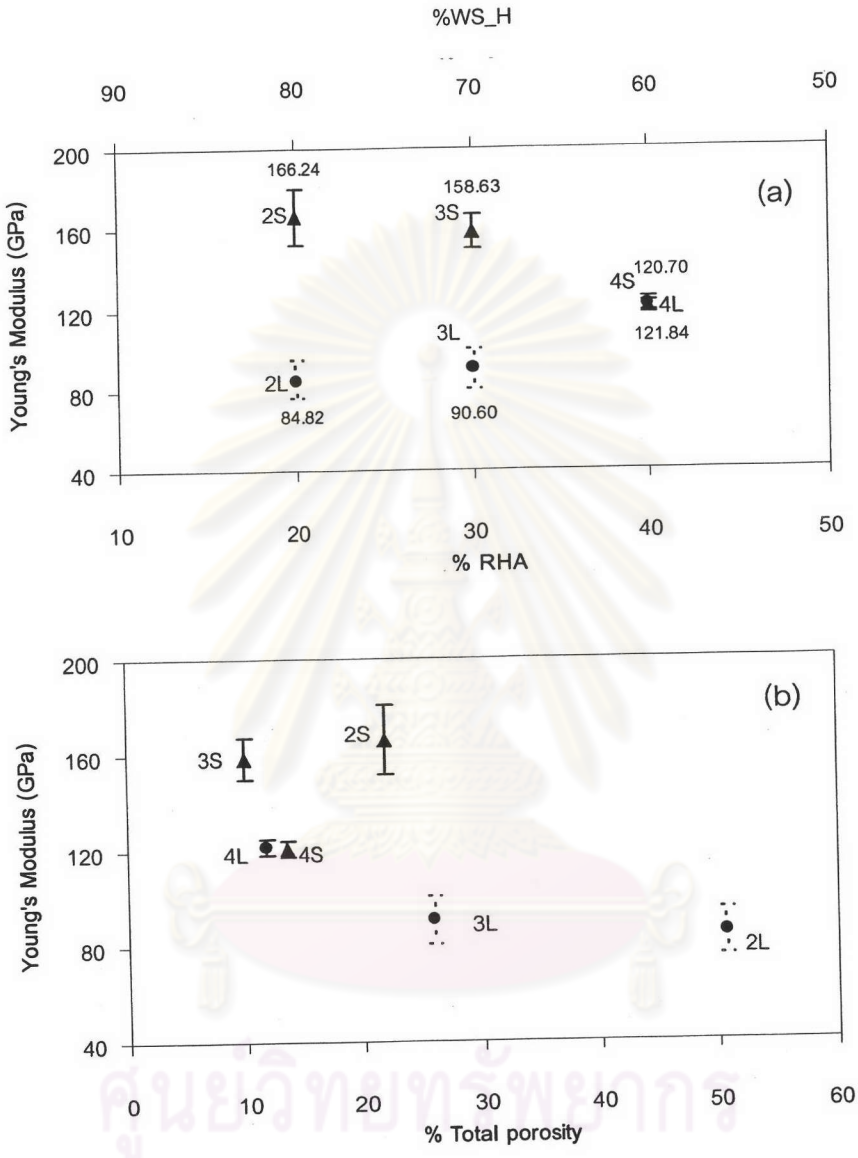

Figure 4.34 Young's modulus of specimens fired at 1700 °C for 1 hour.

Flexural strength are not significantly different among 2S, 3S and 4S samples. But when compare between the samples made from different size precursors. However, those smaller size precursors have superior strength to the others. The strength of the samples in this study is influenced by % porosity (Figure 4.36 (a))

Similarly to the hardness, 2S, 3S and 4S generally show higher hardness than 2L, 3L and 4L. And the hardness is mainly dependent on % porosity (Figure 4.36 (b)). Among 2S, 3S and 4S, 4S has the lowest hardest because of highest silica content. Whereas 2L, 3L and 4L, the porosity play a major role instead.

Move to the fracture toughness, the toughness of 2L, 3L and 4L are not possible to measure by the indentation technique as crack propagation is obstructed by the pores which intensively spread over. Only the value of 2S, 3S and 4S are available for the consideration. Assumable, the samples from large precursors which are more porous are less tough than the others as found

When consider among the sample from small size precursors, 2S samples contain alumina K_C = 2.0-6.0 MPa.$m^{1/2}$ that has higher fracture toughness than mullite K_C = 2.0-4.0 MPa.$m^{1/2}$. The fracture toughness of 2S is comparable to 3S. 4S has the excessive silica in the composition, its fracture toughness is lowest (Figure 4.35 (c)) because glassy phase can not retard crack propagation. It is believed that glassy phase influences to fracture toughness more than % total porosity as shown in Figure 4.36 (c).

Particle size of the precursors may influence crystallization, crystal growth and thus the final properties. Further investigation is needed to clarify this influence.

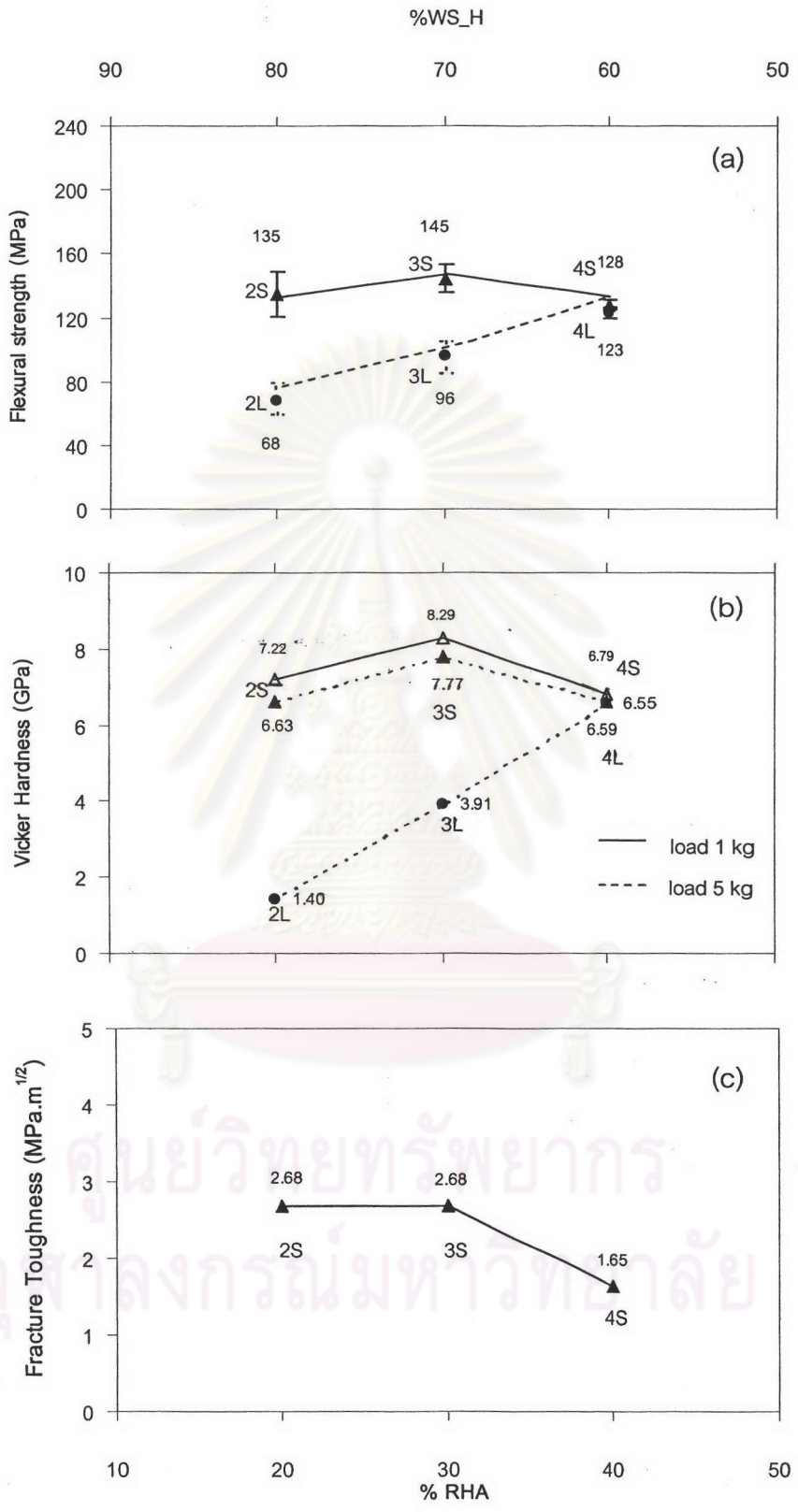

Figure 4.35 Flexural strength, Vicker hardness and fracture toughness of specimens fired at 1700 °C for 1hour.

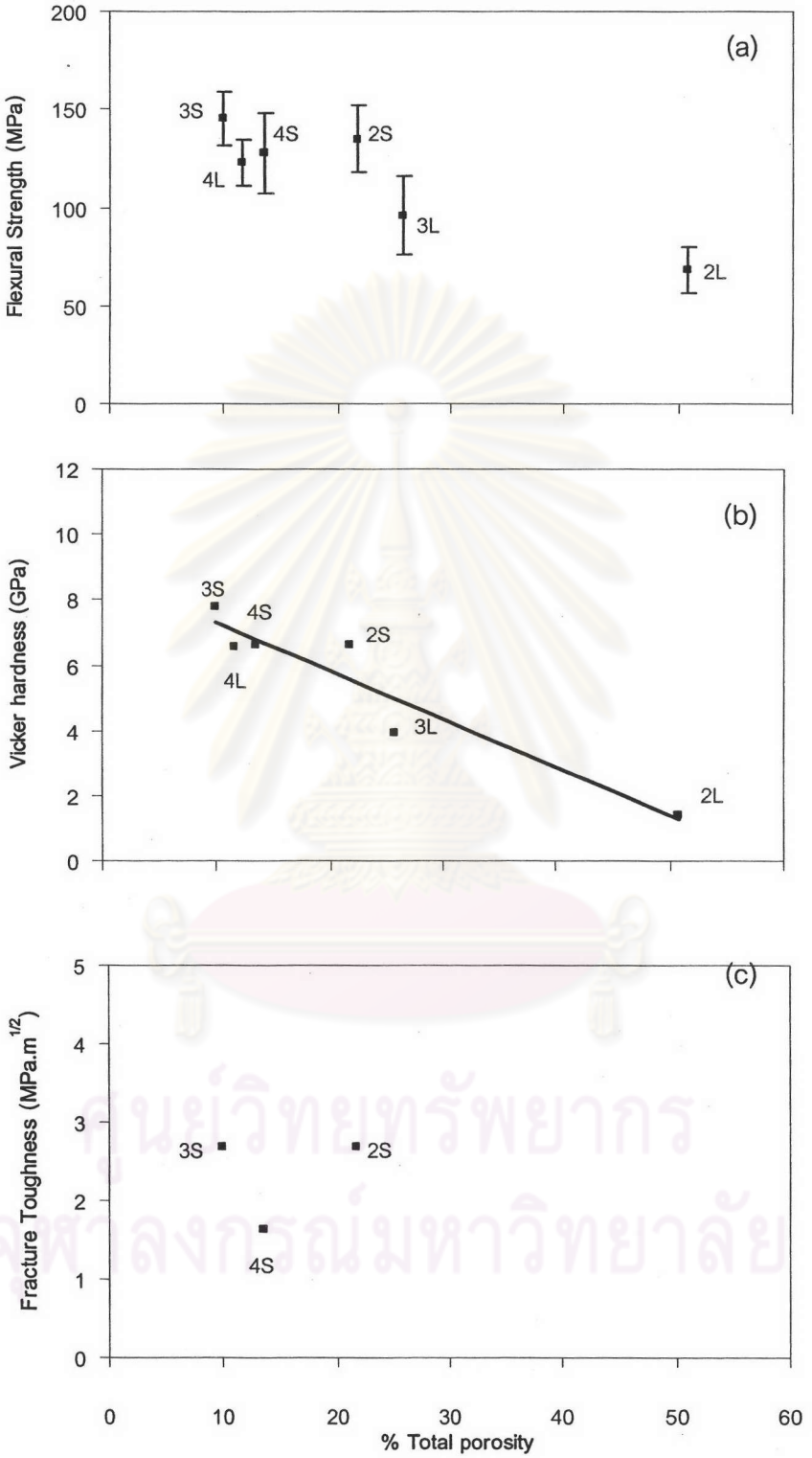

Figure 4.36 Flexural strength, Vicker hardness, fracture toughness and % total porosity of specimens fired at 1700 °C for 1 hour.

4.4.3.4 Thermal properties

Coefficients of thermal expansion (CTE) of 4S, 3S and 2S are slightly different 6.82, 6.39 and 6.64 x10^{-6}/°C, respectively (Figure 4.37). 3S has the lowest CTE attributable to highest amount of mullite, which is the interlock structure and low movement in the structure when temperature increases.

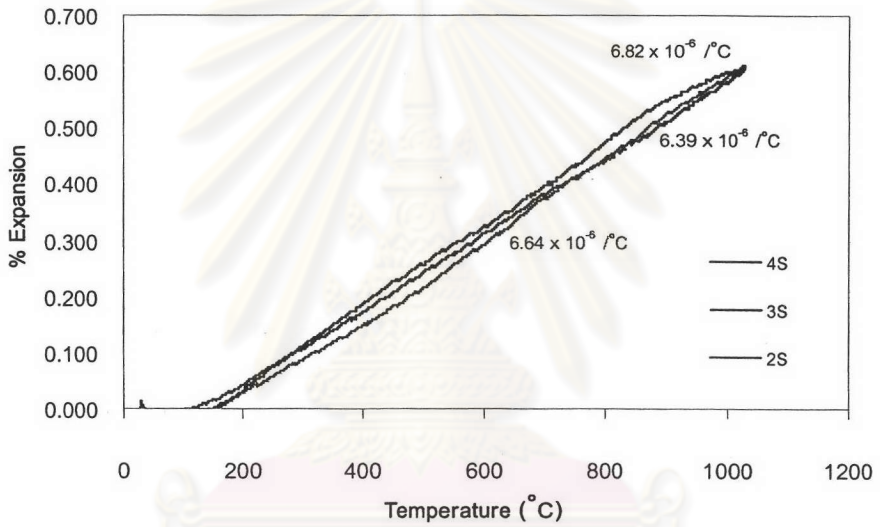

Figure 4.37 Coefficient of thermal expansion of specimens fired at 1700 °C for 1 hour.

Most of samples has the thermal shock resistance ΔT= 250 °C (Figure 4.38). Their flexural strengths start to fall at ΔT= 250 °C. 4S and 4L have the similar structure therefore their thermal shock resistances are identical. Flexural strength of 2S dramatically drops at ΔT= 250 °C because it has more Al_2O_3 content which has higher CTE than mullite.

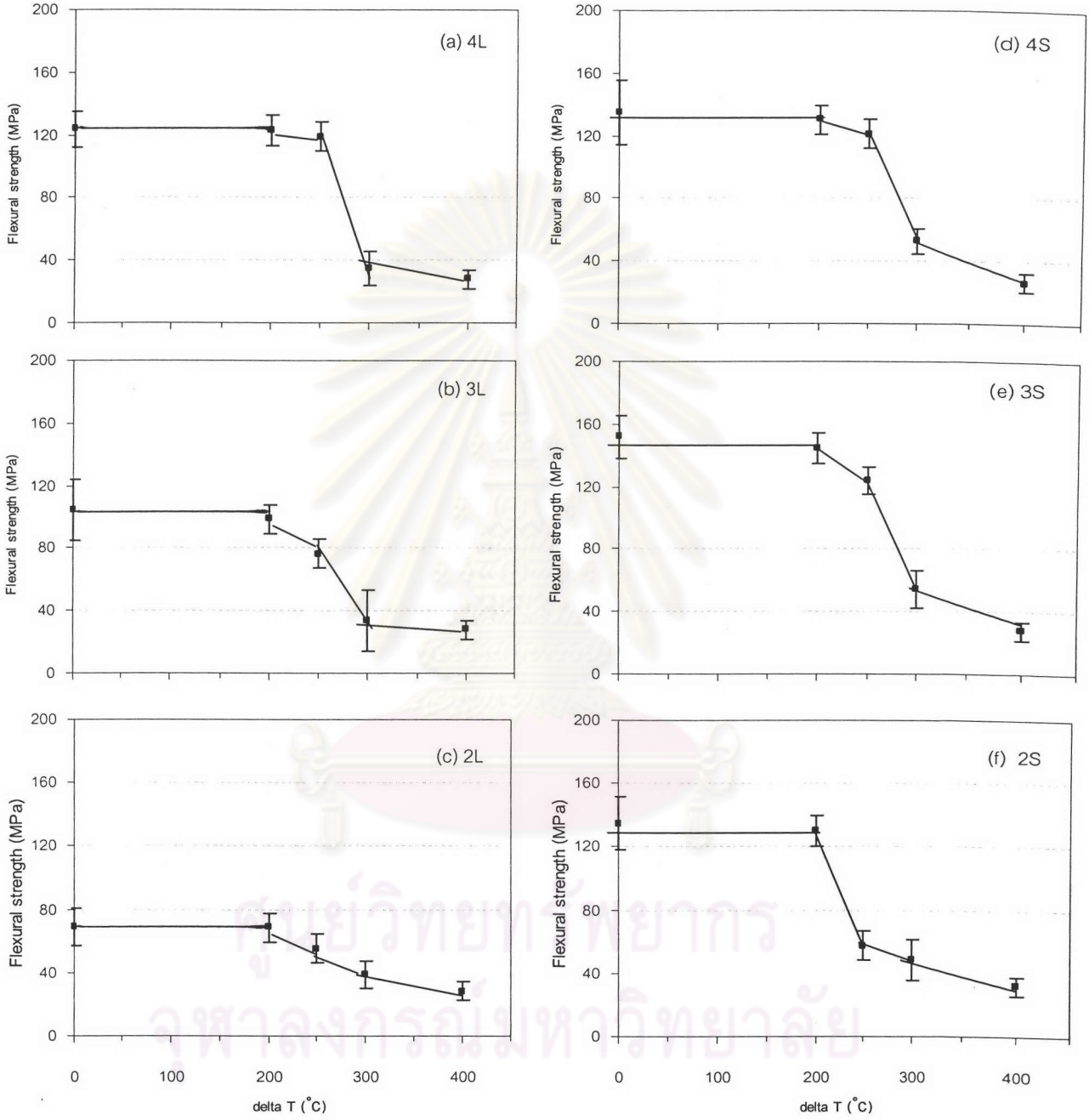

Figure 4.38 Thermal shock resistance of specimens fired at 1700 °C for 1 hour.

The properties of 3S is comparable to commercial slip casting mullite (Table 4.11).

Table 4.11 Properties of 3S sample and commercial mullite grade products.

Properties	Mullite products	
	RHA/WS_H	Commercial [48]
Physical properties		
- Bulk density (g/cm^3)	2.8	2.8
- % Water absorption	0.09	0
Mechanical properties		
- Young's Modulus (GPa)	159	150
- Flexural Strength (MPa)	145	170-180
- Vickers Hardness (GPa)	7.8 (5 kg load)	10
- Fracture Toughness ($MPa.m^{1/2}$)	2.7	2.0
Thermal properties		
- Coefficient of Thermal Expansion ($x10^{-6}/°C$)	6.4	5.3-5.4
- Thermal Shock ΔT (°C)	250	300
- Maximum Use Temperature (°C)	1600	1700